

Response of linear-elastic structures to near-fault ground motions

2012

Kristján Ingvi Ólason

Master of Science in Civil Engineering



Response of linear-elastic structures to near-fault ground motions

Kristján Ingvi Ólason

Id no: 310581-5939

Master of Science

Civil Engineering

May 2012

School of Science and Engineering

Reykjavík University



Response of linear-elastic structures to near-fault ground motions

Kristján Ingvi Ólason

Thesis (30 ECTS) submitted to the School of Science and Engineering
at Reykjavík University in partial fulfillment
of the requirements for the degree of
Master of Science in Engineering

May 2012

Supervisor(s):

Ph.D. Rajesh Rupakhety, Supervisor
Assistant Research Professor, University of Iceland

Ph.D. Jónas Þór Snæbjörnsson, Co-Supervisor
Professor, Reykjavík University

Examiner:

Ph.D. Candidate Sigurður Unnar Sigurðsson, Examiner
Earthquake Engineering Research Center, University of Iceland



Línuleg-elastísk svörun stálramma vegna nálægðaráhrifa jarðskjálfta

Kristján Ingvi Ólason

Ritgerð (30 ECTS) lögð fram við tækni- og verkfræðideild
Háskólans í Reykjavík til
meistaraprófs (MSc)

Maí 2012

Leiðbeinandi/leiðbeinendur:

Ph.D. Rajesh Rupakhety, Supervisor
Assistant Research Professor, University of Iceland

Ph.D. Jónas Þór Snæbjörnsson, Co-Supervisor
Professor, Reykjavík University

Prófdómari:

Ph.D. Candidate Sigurður Unnar Sigurðsson, Examiner
Earthquake Engineering Research Center, University of Iceland

Copyright

Kristján Ingvi Ólason

May 2012

The undersigned hereby certify that they recommend to the School of Science and Engineering at Reykjavík University for acceptance this project report entitled *Response of linear-elastic structures to near-fault ground motions* submitted by Kristján Ingvi Ólason in partial fulfilment of the requirements for the degree of Master of Science in Civil Engineering.

Date

Ph.D. Candidate Sigurður Unnar Sigurðsson, Examiner
Earthquake Engineering Research Center, University of Iceland

Ph.D. Rajesh Rupakhety, Supervisor
Assistant Research Professor, University of Iceland

Ph.D. Jónas Þór Snæbjörnsson, Co-Supervisor
Professor, Reykjavík University

The undersigned hereby grants permission to the Reykjavík University Library to reproduce single copies of this project report entitled *Response of linear-elastic structures to near-fault ground motions* and to lend or sell such copies for private, scholarly or scientific research purposes only.

The author reserves all other publication and other rights in association with the copyright in the project report, and except as herein before provided, neither the project report nor any substantial portion thereof may be printed or otherwise reproduced in any material form whatsoever without the author's prior written permission.

Date

Kristján Ingvi Ólason
Master of Science

Abstract

Recorded earthquake ground motions in the near-fault regions have different and peculiar characteristics compared to that in the far-fault region. The main difference is a strong long period pulse in the velocity record due to forward directivity effects. This phenomenon can cause severe damage to flexible structures like high rise buildings. Seismic design codes are based on far-fault ground motion data and provisions for structures in near-fault regions are inadequate. In this study the main characteristics of near-fault ground motions are addressed. Time-history analyses are performed for linear-elastic steel frames of five different heights. The dataset used in this study contains acceleration records from 27 different earthquakes with total of 56 records. The near-fault strong-motion dataset used in this study was collected and processed by Rupakhety (2010). The time-history results of equivalent static storey forces for the frames differed increasingly from the linear distribution of equivalent static storey force method in EC8, as the total height of the frames increased. The Eurocode 8 (EC8) storey force distribution approximates the dynamic behaviour by considering only a single mode. Results from time history analysis suggests that for near-fault sites the linear distribution of equivalent static storey forces in EC8 might not satisfy the actual storey forces for the lower half of tall structures but for the upper half of structures the provision is excessive. Two models of storey force distribution are proposed for near-fault ground motion areas obtained by fitting a 5th and 3rd degree polynomials to the mean storey force distribution obtained from time-history analysis. The simpler of the two proposed models is tested with examples and proves to simulate storey forces better than the EC8 storey force method which is based on the response of the fundamental period of a structure.

Keywords: near-fault ground motion, forward directivity, time-history analyses, equivalent static storey forces, linear-elastic seismic response.

Útdráttur

Yfirborðshreyfingar vegna jarðskjálfta nálægt upptökum skjálfta (e. near-fault region) eru ólíkar þeim hreyfingum sem eiga sér stað lengra frá upptökunum (e. far-fault region). Meginmunurinn er sterkur langur púls í yfirborðs hraðamælingum vegna afgerandi stefnubundinna þátta (e. forward directivity). Þetta fyrirbrigði getur valdið miklum skemmdum á sveigjanlegum burðarkerfum eins og háum byggingum. Jarðskjálftastaðlar byggja á jarðskjálftamælingum sem gerðar eru langt frá upptökum jarðskjálfta, en staðlarnir eru ófullnægjandi fyrir byggingar sem staðsettar eru nærri upptökusvæðum jarðskjálfta. Í þessu verkefni eru aðaleinkenni nærsviðsáhrifa (e. near fault) skoðuð. Tímaraðagreining er framkvæmd fyrir línulega svörun fimm mishárra stálramma. Við tímaraðagreininguna er notast við gagnasafn sem inniheldur hröðunarsögu (e. acceleration record) 27 ólíkra jarðskjálfta og í heild 56 hröðunarsögur. Gagnasafninu var safnað saman og unnið af Rupakhety (2010). Niðurstöður tímaraðagreiningarinnar sýna að eftir því sem heildarhæð rammanna jókst, viku jafngildandi kraftar á hæðarskilum rammanna í auknum mæli frá þeirri línulegu dreifingu á jafngildandi kröftum á hæðarskilum sem gefin eru upp í Eurocode 8 (EC8). Í EC8 er gert ráð fyrir að kraftadreifing á hæðarskilum verði einungis í einu sveifluformi. Niðurstöður tímaraðagreininganna benda hins vegar til þess að á svæðum þar sem nærsviðsáhrifa gætir er aðferð EC8 ekki að uppfylla raunverulega kraftadreifingu í neðri hluta hárra bygginga en kraftadreifingunni er ofaukið í efri hlutanum. Í verkefninu er því gerð tillaga að tveimur líkönum fyrir kraftadreifingu í hæðarskilum fyrir nærsviðsáhrifasvæði en þau eru fengin með því að fella fimmta og þriðja stigs margliðu að meðal kraftadreifingu í hæðarskilum sem fengin eru frá tímaraðagreiningunum. Einfaldara líkanið er prófað með notkun dæma og reynist líkja eftir kröftum í hæðarskilum betur en aðferð EC8 sem er byggð á svörun grundvallar sveiflutíma bygginga.

Lykilorð: nærsviðsáhrif, stefnuáhrif, tímaraðagreining, jafngildandi kraftar í hæðarskilum, línuleg jarðskjálftasvörun.

Acknowledgements

I would first and foremost like to thank Dr. Rajesh Rupakhety for great teaching and for accepting to be my M.Sc. thesis supervisor. This project was based on Dr. Rupakhety's suggestion for thesis and it was an honour and privilege to work under his supervision.

I thank Dr. Jónas Þór Snæbjörnson Co-Supervisor for reading the manuscript and giving valuable comments for the project.

I would also like to thank everyone at the Earthquake Engineering Research Centre of University of Iceland at Selfoss for allowing me to work on the thesis at their facilities which gave invaluable time with Dr. Rupakhety.

Finally I want to dedicate this thesis to my dear Gyða Mjöll Ingólfssdóttir

Table of Contents

LIST OF FIGURES.....	II
LIST OF TABLES.....	IV
1 INTRODUCTION.....	1
1.1 BACKGROUND AND PROBLEM STATEMENT	1
1.2 HYPOTHESIS, AIM AND OBJECTIVE OF THIS STUDY	1
1.3 SCOPE OF THE PROJECT	2
2 NEAR-FAULT GROUND MOTION.....	3
2.1 BACKGROUND.....	3
2.2 NEAR-FAULT GROUND MOTION CHARACTERISTICS	4
2.2.1 <i>Effect of directivity.....</i>	4
2.2.2 <i>Fling effect.....</i>	6
2.2.3 <i>Hanging wall effect.....</i>	7
2.2.4 <i>Interface or surface pressure-wave effect.....</i>	7
3 NEAR-FAULT GROUND MOTION RECORDS USED IN THIS STUDY.....	8
4 TIME-HISTORY ANALYSIS OF LINEAR-ELASTIC STEEL FRAMES.....	11
4.1 STRUCTURAL PROPERTIES	11
4.1.1 <i>Geometrical properties</i>	11
4.1.2 <i>Inertial properties of the structures</i>	12
4.1.3 <i>Distribution of stiffness along the height of the building</i>	12
4.2 DAMPING IN THE FRAME MODELS.....	14
4.3 ELASTIC AND DAMPING PROPERTIES OF THE GENERIC FRAMES.....	15
4.3.1 <i>Modal periods, effective modal mass, modal damping ratios.....</i>	15
4.3.2 <i>Mode shapes of the generic frames.....</i>	18
4.4 MODAL ANALYSIS.....	23
4.5 TIME-HISTORY ANALYSIS AND FEM SOLUTIONS.....	25
4.5.1 <i>Computation of shear forces.....</i>	26
4.5.2 <i>Computation of storey forces.....</i>	26
5 RESULTS AND DISCUSSION	29
5.1 MODEL RESULTS COMPARED WITH EC8 PROVISIONS	36
5.1.1 <i>Difference of storey force results and EC8 provisions due to predominant period.....</i>	39
5.1.2 <i>Difference of storey force results and EC8 provision at specific heights</i>	46
6 A NEW MODEL FOR STOREY FORCE DISTRIBUTION IN NEAR-FAULT REGIONS	49
6.1.1 <i>Effect of Normalized pulse period on mean time-history storey force response of frames</i>	53
6.1.2 <i>Comparison of mean time-history results, proposed model II and EC8 provision</i>	57
7 CONCLUSIONS	61
7.1 FINAL REMARKS.....	63
8 REFERENCES.....	64
9 APPENDIX:.....	66

List of Figures

Figure 2.1: Regional map of the rupture at Landers earthquake 1992. The recording stations at opposite ends of the fault are shown and the epicentre. The direction of propagation and the recorded velocity time histories show the forward and backward directivity (Somerville 1997).	6
Figure 3.1: Ground velocity time-history, San Fernando, CA, USA – 1971, WID 1 in dataset used in this study (see dataset metadata in Table 9.1 in Appendix).	9
Figure 3.2: Ground velocity time-history, South Iceland – 2000, WID 88 in dataset used in this study (see dataset metadata in Table 9.1 in Appendix).	9
Figure 3.3: Ground velocity time-history, Ölfus, South Iceland – 2008, WID 92 in dataset used in this study (see dataset metadata in Table 9.1 in Appendix).	10
Figure 4.1: Generic one-bay 6, 9, 12, 15 and 18-storey frames used in this study. Each storey has a height of 3.66 m = 12 feet and a bay length of 7.32 m = 24 feet.	12
Figure 4.2: First five mode shapes of the six storey frame.	18
Figure 4.3: First five mode shapes of the nine storey frame.	19
Figure 4.4: First five mode shapes of the nine storey frame.	20
Figure 4.5: First five mode shapes of the fifteenth storey frame.	21
Figure 4.6: First five mode shapes of the eighteenth storey frame.	23
Figure 4.7: Illustration example of equivalent external storey forces (F_i) from shear forces (V_i). The sum of storey forces is equal to the base shear (V_1) referred to as F_b in EC8.	27
Figure 5.1: Velocity response spectra of the 56 records (log-log plot) are shown as grey lines. The fundamental periods of the frames are shown as the red dash dot lines (see fundamental periods of the frames in table 4.3).	29
Figure 5.2: Plot of normalized storey forces along normalized height for the 6 storey frame structure. The absolute maximum of the 56 records are shown as grey lines. The mean values of the 56 records are shown as a blue line.	32
Figure 5.3: Plot of normalized storey forces along normalized height for the 9 storey frame structure. The absolute maximum of the 56 records are shown as grey lines. The mean values of the 56 records are shown as a blue line.	32
Figure 5.4: Plot of normalized storey forces along normalized height for the 12 storey frame structure. The absolute maximum of the 56 records are shown as grey lines. The mean values of the 56 records are shown as a blue line.	33
Figure 5.5: Plot of normalized storey forces along normalized height for the 15 storey frame structure. The mean values of the 56 records are shown as a blue line. The absolute maximum of the 56 records are shown as grey lines. The mean values of the 56 records are shown as a blue line.	33
Figure 5.7: Mean values of normalized storey forces for all the frame structures compared with EC8 normalized provision for storey forces.	36
Figure 5.8: Mean values of normalized storey forces for all six frames, normalized with the storey force at roof, compared with EC8 normalized provision for storey forces.	37
Figure 5.9: Mean for all the frames in one curve compared with EC8 provision for storey forces.	38
Figure 5.10: Mean storey forces for each normalized period group plotted with all maximum absolute storey forces and EC8 storey force distribution for the 6 storey frame.	40
Figure 5.11: Mean storey forces for each normalized period group plotted with all maximum absolute storey forces and EC8 storey force distribution for the 9 storey frame.	41
Figure 5.12: Mean storey forces for each normalized period group plotted with all maximum absolute storey forces and EC8 storey force distribution for the 12 storey frame.	41
Figure 5.13: Mean storey forces for each normalized period group plotted with all maximum absolute storey forces and EC8 storey force distribution for the 15 storey frame.	42
Figure 5.14: Mean storey forces for each normalized period group plotted with all maximum absolute storey forces and EC8 storey force distribution for the 18 storey frame.	42

Figure 5.15: Plot of the mean difference of absolute normalized storey forces between near-fault modelling and normalized EC8 provisions for a 6 storey structure.	43
Figure 5.16: Plot of the mean difference of absolute normalized storey forces between near-fault modelling and normalized EC8 provisions for a 9 storey structure.	44
Figure 5.17: Plot of the mean difference of absolute normalized storey forces between near-fault modelling and normalized EC8 provisions for a 12 storey structure.	44
Figure 5.18: Plot of the mean difference of absolute normalized storey forces between near-fault modelling and normalized EC8 provisions for a 15 storey structure.	45
Figure 5.19: Plot of the mean difference of absolute normalized storey forces between near-fault modelling and normalized EC8 provisions for an 18 storey structure.	45
Figure 5.20: Difference of all near-fault ground motions storey forces and EC8 distribution as a function of normalized period T_n at height 1/3 of the 6,9,12,15 and 18 storey frames.	46
Figure 5.21: Difference of all near-fault ground motions storey forces and EC8 distribution as a function of normalized period T_n at height 2/3 of the 6,9,12,15 and 18 storey frames.	47
Figure 5.22: Difference of all near-fault ground motions storey forces and EC8 distribution as a function of normalized period T_n at height 3/3 of the 6,9,12,15 and 18 storey frames.	47
Figure 6.1: Proposed model I fitted to the mean time-history storey force results for all the frames and EC8 model.	51
Figure 6.2: Proposed model II fitted to the mean time-history storey force results for all the frames and EC8 model.	51
Figure 6.3: Proposed model II compared with the mean time-history results for the six storey frame. Effects of T_n groups to the storey force response shown along.	53
Figure 6.4: Proposed model II compared with the mean time-history results for the nine storey frame. Effects of T_n groups to the storey force response shown along.	54
Figure 6.5: Proposed model II compared with the mean time-history results for the twelve storey frame. Effects of T_n groups to the storey force response shown along.	54
Figure 6.6: Proposed model II compared with the mean time-history results for the fifteen storey frame. Effects of T_n groups to the storey force response shown along.	55
Figure 6.7: Proposed model II compared with the mean time-history results for the eighteen storey frame. Effects of T_n groups to the storey force response shown along.	56
Figure 6.8: Proposed model II compared with the mean time-history results and EC8 storey force method.	57
Figure 6.9: Proposed model II compared with the mean time-history results and EC8 storey force method.	58
Figure 6.10: Proposed model II compared with the mean time-history results and EC8 storey force method.	59
Figure 6.11: Proposed model II compared with the mean time-history results and EC8 storey force method.	59
Figure 6.12: Proposed model II compared with the mean time-history results and EC8 storey force method.	60

List of Tables

Table 4.1: Second moment of inertia of the beams at each storey of the 6, 9, 12, 15 and 18-storey frames used in the study. In each storey the second moment of inertia of the beam and the column are equal.....	13
Table 4.2: Values of a_0 and a_1	14
Table 4.3: Modal vibration periods of the 6, 9, 12, 15 and 18-storey generic frames used in the study.....	15
Table 4.4: Effective modal mass for the 6, 9, 12, 15 and 18-storey generic frames used in the study.	16
Table 4.5: Modal damping ratios of the 6, 9, 12, 15 and 18-storey generic frames used in the study.....	17
Table 4.6: First 5 mode shapes of the 6-storey frame.....	18
Table 4.7: First 5 mode shapes of the 9-storey frame.....	19
Table 4.8: First 5 mode shapes of the 12-storey frame.....	20
Table 4.9: First 5 mode shapes of the 15-storey frame.....	21
Table 4.10: First 5 mode shapes of the 18-storey frame.....	22
Table 5.1: Modelled mean maximum absolute storey forces for all the frames.	30
Table 5.2: Modelled mean maximum absolute storey forces as percentage of base shear for all the frames.	31
Table 5.3: Fundamental periods of the frames.....	39
Table 5.4: Number of records in each T_n group for each frame.....	40
Table 9.1: The near fault (56 records) dataset metadata. The dataset was collected and processed by Rupakhety <i>et al.</i> (2010).....	66

1 Introduction

1.1 Background and Problem statement

This M.Sc. project is in the field of earthquake engineering. This project is a study of structural response to ground-motion in the near-fault area.

Recorded earthquake ground motions in the near-fault regions have different and peculiar characteristics compared to those in the far-fault region. The main difference is a strong, long period pulse in the velocity record due to forward directivity effects. This phenomenon can cause severe damage to flexible structures like high rise buildings.

Seismic design codes are based on far-fault ground motion data and provisions for structures in near-fault regions are inadequate. Near-fault ground motions are known to have caused severe damage to engineering structures like in the 1995 Northridge, 1995 Kobe and 1999 Chi-Chi earthquakes. Research of near-fault ground motions is therefore important to improve understanding and design provisions for near-fault areas.

1.2 Hypothesis, Aim and Objective of this study

The aim of this study is to analyse the dynamic response of Multi degree of freedom (MDOF) structures due to near-fault ground motions using a dataset of recorded near-fault ground motions containing forward directivity effects.

The main objectives of the study are:

1. Analyse response of generic linear-elastic steel frames of five different heights: 6, 9, 12, 15 and 18 storeys, by time-history analysis using near-fault ground motion dataset of 56 records obtained from 27 different earthquakes.
2. Analyse the story force distribution obtained from time history analysis and compare the results with Eurocode 8 (European Committee for Standardization 2003, (EC8)) provisions.
3. Analyse the effect of the predominant period (T_d) of ground motion on the story force distribution.

4. Propose a model which simulates the distribution of lateral storey forces for near-fault ground motions.

The hypothesis of this project is that the equivalent static storey force distribution in EC8 which approximates the dynamic behaviour by considering only a single mode does not simulate the response for near-fault ground motions adequately.

1.3 Scope of the project

This project is divided into seven separate chapters and appendix. The topics covered in each section are the following:

1. Introduction: In this chapter the general introduction of the research project is covered, including the background, aim and hypothesis of the research. The objectives of the project are listed, and the structure of the report is discussed.
2. Near-fault ground motion: This chapter covers a general introduction to near-fault ground motions and their most important characteristics.
3. Near-fault ground motion records used in this study: The dataset of forward directivity ground motion records, which is used in the time-history analysis, is introduced and outlined.
4. Time-history analysis of linear-elastic steel frames: In this chapter the properties of the modelled structures used in the time-history analysis are presented along with a description of the modal analysis procedure.
5. Results and Discussion: The results are presented and discussed simultaneously along with a comparison to the EC8 recommendations. The effects of the predominant period (T_d) of the ground motions to the response of the frame structures are analysed.
6. A new model for storey force distribution in near-fault regions: Two new models for storey force distribution due to near-fault ground motions are proposed and explained.
7. Conclusion: The main findings and conclusions of this project are summarized.
8. Appendix - The dataset used in this project: The 56 records of the dataset used in this study are presented with the associated metadata.

2 Near-fault ground motion

In this section the near-fault phenomenon is examined and its peculiar characteristics are discussed.

2.1 Background

Benioff (1955) was first to address explanations of the intensity patterns observed in the 1952 Kern County earthquake which was the first seismological evidence for the near-fault phenomenon. Benioff showed that the propagation of fault rupture could lead to different types of ground motions depending on which end of the rupture area the site is located on.

Houser & Trifunac 1967 were the first to observe a time history record where a clear near-fault effect was identified in the Station No.2 (CO2) record acquired from the 1966 Parkfield, California earthquake.

Mahin *et al.* (Mahin, Bertero, Chopra & Collins, 1976) pointed at the nature of structural response due to the large pulse motion in the vicinity of the causative fault.

The destructive effects to flexible structures built in the vicinity of the causative faults due to near-fault effects were first analysed by Bertero *et al.* (Bertero, Mahin & Herrera, 1978) after the 1971 San Fernando earthquake. It was identified that the Olive View Medical centre building suffered structural failure which was described to have been caused by a severe pulse referred to as a characteristic of near-fault ground motion.

Near-fault effects had, however, not received much attention among researchers until the 1994 Northridge and 1995 Hyogo-ken Nanbu (Kobe) earthquakes. The devastating damage and tremendous losses in these densely populated areas due to these earthquakes led to increased recognition of near-fault effects.

Hall *et al.* (1995) pointed out that high-rise and base-isolated buildings designed according to code provisions could experience severe displacement demands due to displacement pulses within the near-fault ground motion.

Iwan (1997) stated that the effect of near-fault earthquakes, even for elastic structures, could not be accounted for by multiplying the code (Uniform Building Code, 1997) prescribed base shear coefficient by a near-fault factor.

2.2 Near-fault ground motion characteristics

Earthquake ground motions recorded in the near-fault region are different in many ways from those recorded at far-field stations. The impulsive characteristic of ground velocity and displacement are the most essential characteristic of near-fault events. Figure 3.1-Figure 3.3, in chapter 3 where the dataset used in this study is introduced, show ground velocity of three records in near-fault region with a strong, long velocity pulse.

Near-fault ground motions can cause more damage to certain types of structures than far-fault ground motions. Especially can these effects be disastrous for flexible structures. A study explaining the characteristics of near-fault ground motions in detail and the possible impact on engineering structures was done by Rupakhety *et al.* (2010).

2.2.1 Effect of directivity

There are three known types of directivity effects that depend on the fault and the direction of rupture propagation along the fault.

2.2.1.1 Forward directivity

When an earthquake occurs, a shear dislocation begins at a point on a fault which spreads at a velocity that is almost equal to the shear wave velocity. A shear wave front is formed by the accumulation of shear waves travelling ahead of the rupture front when such a rupture propagates from the hypocentre. If the site is positioned at one end of the fault and rupture starts at the other end of the fault and travels towards the site, the arrival of the wave front is seen as a large pulse at the beginning of the record (Somerville P. 1997). The conditions that lead to forward rupture directivity effects for strike slip and dip slip faults are the following:

i. Strike slip faults

- Takes place at all locations along the fault away from the hypocenter
- Slip vector points towards the site.
- Rupture spreads towards the site.

ii. Dip slip faults

- The slip direction is aligned upon the fault plane.

- The rupture direction is aligned upon the fault plane.

The shear dislocation on the fault plane causes the pulse to be oriented perpendicular to the fault plane. This causes the fault-normal peak velocity to be much larger than the fault-parallel component. The fault normal components are usually the same for strike-slip faults. The conditions that can cause forward and backward directivity were identified by Somerville, Graves & Abrahamson (1997).

- The smaller the angle between the direction of the rupture propagation and the direction of the waves travelling from the fault to the site the higher the Forward Directivity (FD) effect.
- The larger the fraction of the fault rupture surface that lies between the hypocenter and the site of the surface, the higher the FD effect.
- Forward directivity does not exist if the slip is concentrated near one end of the fault where the station is located even if these geometrical conditions are satisfied.

2.2.1.2 Backward directivity

Ground motion is characterized by a long duration and low amplitude when the rupture propagates away from a site. This effect is known as backward directivity. An example of backward- and forward directivity can be seen in Figure 2.1.

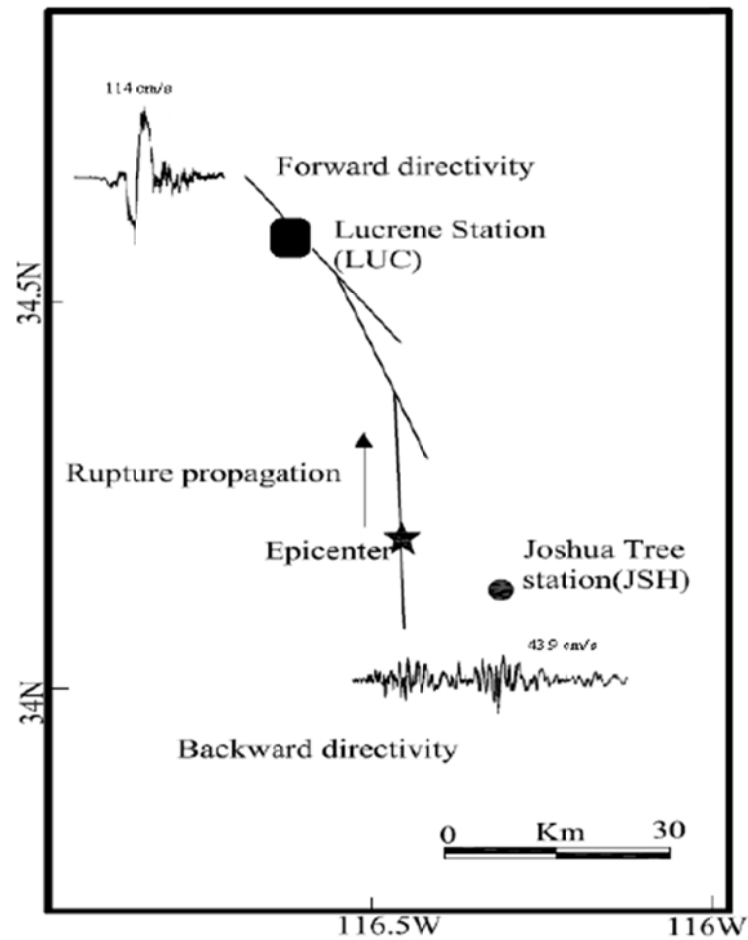


Figure 2.1: Regional map of the rupture at Landers earthquake 1992. The recording stations at opposite ends of the fault are shown and the epicentre. The direction of propagation and the recorded velocity time histories show the forward and backward directivity (Somerville 1997).

2.2.1.3 Neutral directivity

When rupture propagation is neither dominantly towards nor away from a site, the effect is known to be neutral directivity. Depending on magnitude and distance to the fault, these effects can still result in high peak ground acceleration.

2.2.2 Fling effect

Distinct pulses are mainly caused by forward directivity but another effect can also contribute which are known as a fling effect. Permanent tectonic deformations of the ground at a site can cause fling effect during an earthquake, which is observed as a step displacement and one-sided

velocity pulse. When excessive tectonic deformations take place because of a large slip on the fault plane, the fling effect can be significant (Abrahamson, 2000).

2.2.3 Hanging wall effect

Sites located on a hanging wall of a dip-slip fault are known to experience greater ground motion than sites positioned on a foot wall at the same closest distance. After the devastating Mw 6.7, Northridge earthquake of 1994, Abrahamson and Somerville (1996) discovered that the peak horizontal acceleration in the hanging wall stations records were 50% greater than the average peak ground acceleration over a range of 10 to 20 km but stations records on the foot wall were close to the average.

2.2.4 Interface or surface pressure-wave effect

SP-wave effect is a known as a characteristic of near-fault ground motion. This effect is due to a shear wave that originates at the source, but which subsequently propagates along the surface with the P-wave velocity. This type of surface wave effects were suggested to cause the damage patterns observed after the Mw 5.93, 1987 Whittier Narrows, California earthquake (Kawase & Aki, 1990) and the Mw 6.3, 1995 Aigion (AEG station), Greece earthquake (Mavroeidis & Papageorgiou, 2000).

3 Near-fault ground motion records used in this study

The dataset used in this study contains acceleration records from 27 different earthquakes with a total of 56 records. The dataset was collected and processed by Rupakhety *et al* (2010). The reason for selecting 56 records out of the 106 which Rupakhety processed in 2010 is that these 56 records contain a clear and dominant pulse in their velocity time series and are affected by forward directivity effects. More details are given in Rupakhety *et al*. (2010). The dataset contains records which have a predominant frequency that is potentially harmful for the frame structures analysed in this project. Details and metadata of the dataset are presented in Table 9.1 in Appendix. The main features of the dataset are:

- The records are acquired from earthquakes in: USA, Mexico, Turkey, the former USSR, Taiwan, Italy and Iceland.
- The moment magnitude (M_w) range is from 5.0 to 6.93 and the Joyner-Boore distance from 0 to 34.6 km.
- The faulting mechanism is categorized. The dataset is dominated by strike-slip events. Out of the 56 records only two belong to normal-faulting. Thirteen belong to reverse-faulting and seven records are produced by events of oblique faulting.
- In cases where permanent displacement and directivity effects are coupled, the permanent displacement part is removed by subtracting a sine pulse from the acceleration time series, the amplitude and frequency of which is scaled to permanent displacement recovered by a procedure explained in Rupakhety *et al*. (2009).
- The components of ground motion being considered are either the strike-normal or strike-parallel. Most components under consideration are the strike-normal ones as that is the component that in most circumstances adequately describes the fault-normal component.

In Figure 3.1 -Figure 3.3 are plotted the time-history ground velocity trace of three records from the dataset used in this study. These plots display the strong long velocity pulse which is due to forward directivity effects.

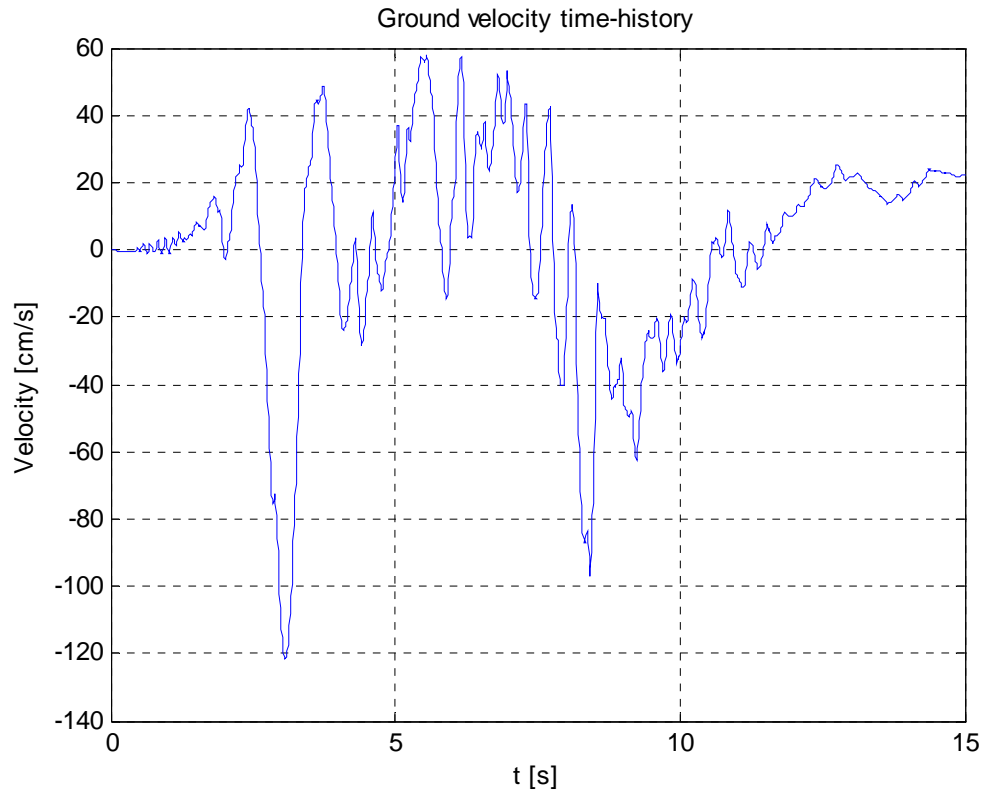


Figure 3.1: Ground velocity time-history, San Fernando, CA, USA – 1971, WID 1 in dataset used in this study (see dataset metadata in Table 9.1 in Appendix).

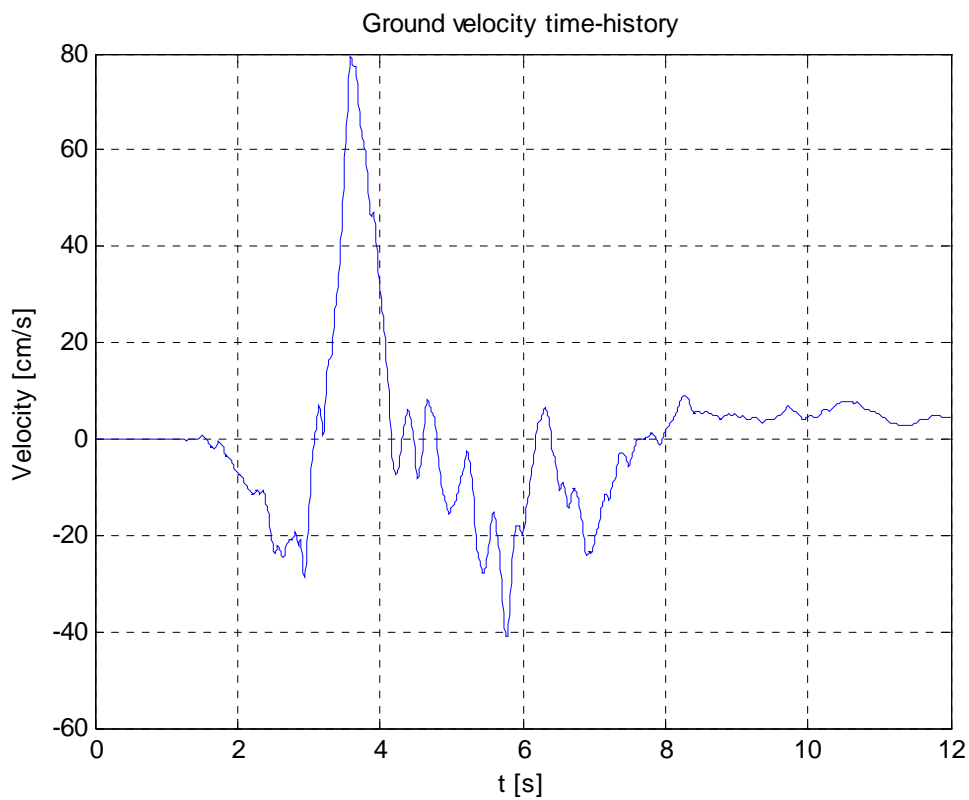


Figure 3.2: Ground velocity time-history, South Iceland – 2000, WID 88 in dataset used in this study (see dataset metadata in Table 9.1 in Appendix).

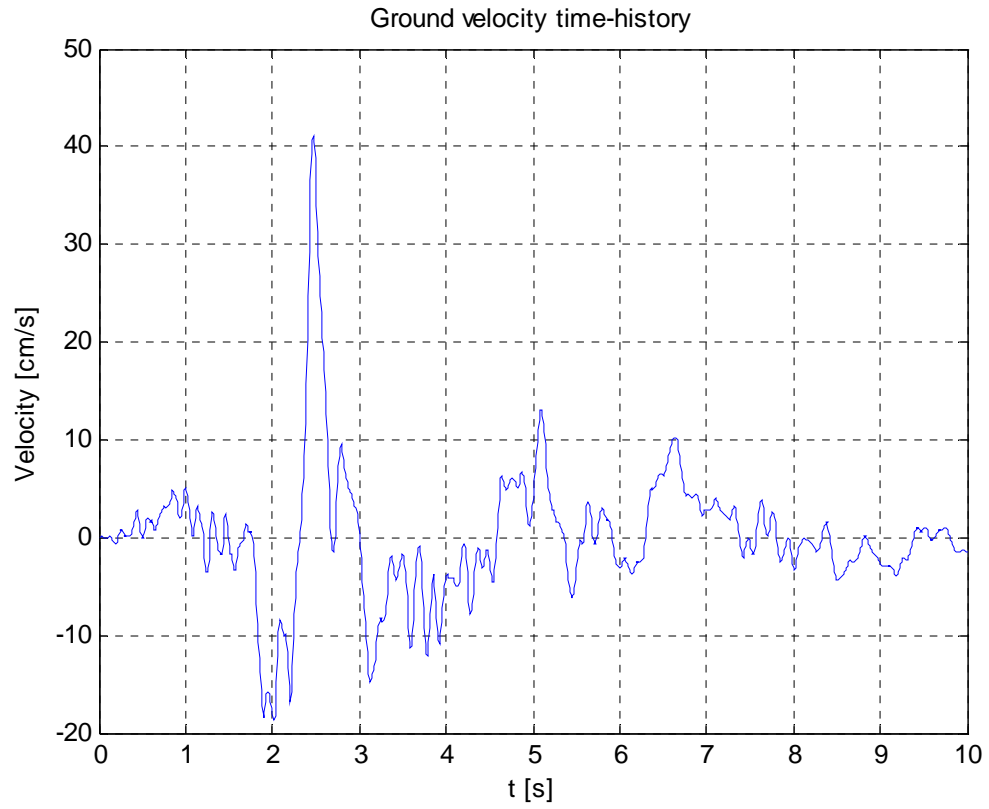


Figure 3.3: Ground velocity time-history, Ölfus, South Iceland – 2008, WID 92 in dataset used in this study (see dataset metadata in Table 9.1 in Appendix).

4 Time-history analysis of linear-elastic steel frames

The structural systems used in this study are single-bay planar moment resisting steel frames. The properties of the modelled frames are the same as were used in Rupakhety (2008). The properties are based on the model of Chintanapakdee and Chopra (2003) which has been used widely by researchers. Further details of the structures considered in this study are provided below.

4.1 Structural properties

Description of the design and modelling is detailed further in the subsequent sections. P-delta effects are not considered in this study. The columns at the ground floor are assumed to be rigidly fixed to the foundation.

4.1.1 Geometrical properties

The frames are a set of generic single-bay frames of six different storeys: 6, 9, 12, 15 and 18. Each storey has a height of 3.66 m = 12 feet and a bay length of 7.32 m = 24 feet. The frames are shown in Figure 4.1.

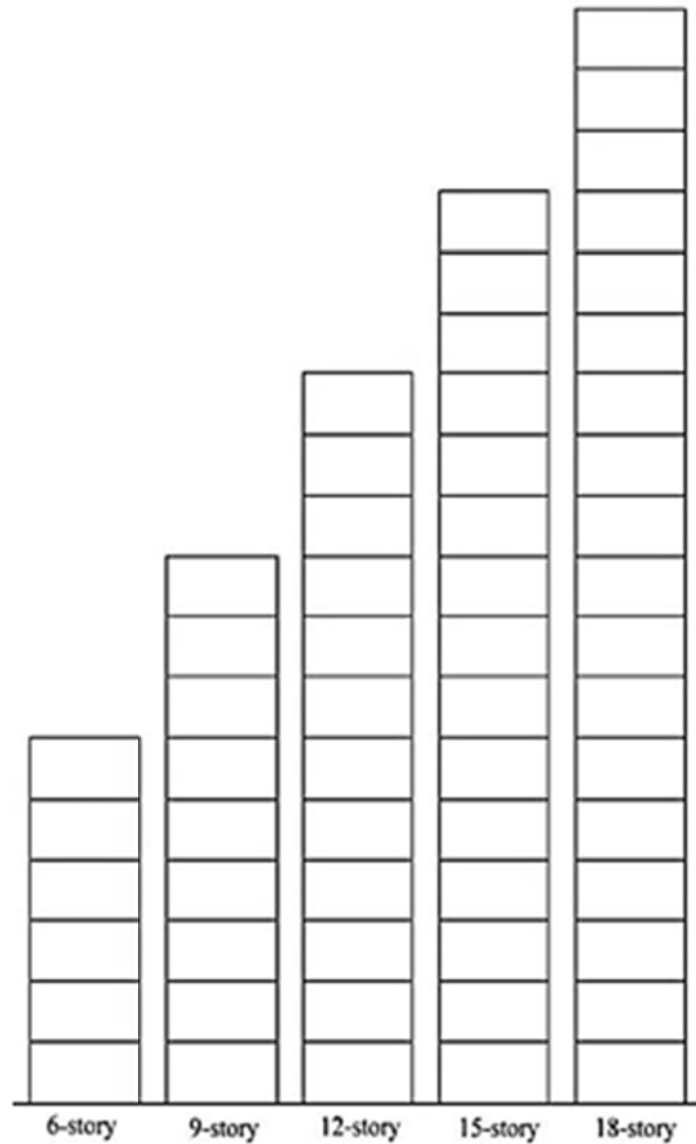


Figure 4.1: Generic one-bay 6, 9, 12, 15 and 18-storey frames used in this study. Each storey has a height of $3.66 \text{ m} = 12 \text{ feet}$ and a bay length of $7.32 \text{ m} = 24 \text{ feet}$.

4.1.2 Inertial properties of the structures

For all the five frames considered in this study, mass equal to $445 \text{ kN} = 100 \text{ kips}$ is assigned as lumped mass at all nodes except nodes at ground level. That gives $890.0 \text{ kN} = 200 \text{ kips}$ mass for every storey. The rotational degrees of freedom (DOFs) are not assigned with any mass.

4.1.3 Distribution of stiffness along the height of the building

The Young's modulus for the steel is assigned 200 GPa . For each storey of the frames the second moment of inertia of the beam in that storey is kept equal to the second moment of

inertia of the two columns supporting the beam. By this assumption the relative values of the stiffness of beams and columns are assigned so as to obtain constant drift along the height of the building when subjected to the lateral forces specified in the International Building code (IBC 2000). When the relative stiffness is distributed for the members of the frames, their absolute values are assigned to have the fundamental period (T_1) given by Equation 1. This equation defines the mean plus one standard deviation of measured periods of steel moment resisting frames (Goel & Chopra, 1997). Equation 1 is only relevant for feet but by multiplying H with 3.2787 it is relevant for meters. The stiffness of the elements is shown in Table 4.1.

$$T_1 = 0.045H^{0.8} \quad (1)$$

Table 4.1: Second moment of inertia of the beams at each storey of the 6, 9, 12, 15 and 18-storey frames used in the study. In each storey the second moment of inertia of the beam and the column are equal.

Storey	$I_{\text{beam}} [\text{m}^4]$				
	6-storey	9-storey	12-storey	15-storey	18-storey
1	0,00081	0,00089	0,00095	0,00102	0,00109
2	0,00279	0,00317	0,00343	0,00369	0,00393
3	0,00141	0,00170	0,00188	0,00203	0,00216
4	0,00145	0,00204	0,00233	0,00254	0,00272
5	0,00092	0,00168	0,00203	0,00225	0,00243
6	0,00042	0,00152	0,00202	0,00230	0,00250
7		0,00120	0,00184	0,00217	0,00241
8		0,00082	0,00166	0,00209	0,00236
9		0,00035	0,00141	0,00194	0,00227
10			0,00111	0,00177	0,00216
11			0,00074	0,00156	0,00203
12			0,00032	0,00131	0,00187
13				0,00101	0,00169
14				0,00067	0,00147
15				0,00028	0,00122
16					0,00093
17					0,00061
18					0,00026

4.2 Damping in the frame models

The frame structures are assumed to have Rayleigh damping. The damping is therefore a sum of a mass proportional component and a stiffness proportional component. The damping matrix is obtained with Equation 2.

$$C = a_0 M + a_1 K \quad (2)$$

Where M is the mass matrix and K is the stiffness matrix. a_0 and a_1 are two constants that can be determined by the modal damping ratios ξ_i , and ξ_j for any two modes i and j . The constants a_0 and a_1 can be found by solving two simultaneous equations. If two modes are assumed to have equal damping ratios ξ and ω_i and ω_j are the natural frequencies corresponding to these modes then a_0 and a_1 can be solved with Equations 3 and 4.

$$a_0 = \xi \frac{2\omega_i\omega_j}{\omega_i + \omega_j} \quad (3)$$

$$a_1 = \frac{2\xi}{\omega_i + \omega_j} \quad (4)$$

In this study the same values of a_0 and a_1 are used as in Rupakhety (2008) where the modal damping ratios in the first and the j^{th} mode were 5%. The j^{th} mode was selected by an iterative procedure so to have weighted average of the modal damping ratios as close to 5% as possible. The values are shown in Table 4.2.

Table 4.2: Values of a_0 and a_1

No. of storeys	a_0	a_1
6	0,378643	0,003725
9	0,269883	0,005580
12	0,226577	0,005159
15	0,188581	0,006366
18	0,162444	0,007517

4.3 Elastic and damping properties of the generic frames

In this section the elastic modal periods, effective modal mass, mode shapes and modal damping ratios of the generic frames are presented.

4.3.1 Modal periods, effective modal mass, modal damping ratios

The modal vibration periods of the 6, 9, 12, 15 and 18-storey generic frames used in this study are presented in Table 4.3. The effective modal mass for each of the generic frames used in this study are presented in Table 4.4. The effective modal masses were obtained with modal mass participation factors that were used to compute the weighted average of the modal damping ratios which are obtained by assuming Rayleigh damping so that the weighted average of the modal damping ratios is as close to 5% as possible. The modal damping ratios for the generic frames used in this study are presented in Table 4.5.

Table 4.3: Modal vibration periods of the 6, 9, 12, 15 and 18-storey generic frames used in the study.

Mode(n)	Modal vibration period T_n (sec)				
	Number of storeys				
	6	9	12	15	18
1	1,379	1,910	2,411	2,892	3,362
2	0,512	0,724	0,914	1,099	1,279
3	0,282	0,423	0,548	0,668	0,782
4	0,173	0,280	0,375	0,465	0,551
5	0,117	0,198	0,274	0,346	0,415
6	0,086	0,145	0,208	0,268	0,326
7		0,112	0,163	0,214	0,264
8		0,091	0,131	0,174	0,217
9		0,075	0,108	0,144	0,182
10			0,092	0,122	0,155
11			0,079	0,105	0,133
12			0,069	0,091	0,116
13				0,081	0,102
14				0,072	0,091
15				0,065	0,082
16					0,074
17					0,068
18					0,067

The effective modal mass of mode i can be solved with Equation 5.

$$M_i^* = \frac{\{r\}^T [M] \{\phi_i\} \{\phi_i\}^T [M] \{r\}}{\{\phi_i\}^T [M] \{\phi_i\}} \quad (5)$$

Where $\{r\}$ is the influence vector, $[M]$ is the mass matrix and $\{\phi_i\}$ is the i^{th} mode shape. The effective modal mass is independent of the mode normalization and shows how much of the total mass participates in each vibrational mode of the structure.

Table 4.4: Effective modal mass for the 6, 9, 12, 15 and 18-storey generic frames used in the study.

Mode(n)	Effective model mass participation factors, MPn [% of total mass]				
	Number of storeys				
	6	9	12	15	18
1	82,01	80,88	80,41	79,84	79,32
2	11,12	10,70	10,40	10,37	10,44
3	3,85	4,05	4,01	4,00	4,00
4	1,64	1,93	2,03	2,08	2,11
5	1,01	1,01	1,15	1,22	1,27
6	0,38	0,63	0,68	0,77	0,82
7		0,46	0,44	0,50	0,55
8		0,25	0,33	0,34	0,38
9		0,09	0,26	0,25	0,27
10			0,17	0,21	0,20
11			0,09	0,17	0,16
12			0,03	0,12	0,14
13				0,08	0,12
14				0,04	0,09
15				0,02	0,06
16					0,04
17					0,02
18					0,00

Table 4.5: Modal damping ratios of the 6, 9, 12, 15 and 18-storey generic frames used in the study.

Mode(n)	Modal damping ratios, ξ_n (%)				
	Number of storeys				
	6	9	12	15	18
1	5,0	5,0	5,0	5,0	5,0
2	3,8	4,0	3,4	3,5	3,5
3	5,0	5,1	3,9	4,0	4,0
4	7,3	6,9	5,0	5,0	5,0
5	10,3	9,3	6,4	6,3	6,2
6	13,9	12,4	8,2	7,9	7,7
7		15,8	10,3	9,7	9,3
8		19,6	12,7	11,7	11,1
9		23,6	15,2	14,1	13,2
10			17,9	16,6	15,5
11			20,7	19,2	17,9
12			23,6	22,0	20,6
13				24,9	23,3
14				27,8	26,1
15				30,7	29,0
16					31,9
17					34,9
18					35,1

4.3.2 Mode shapes of the generic frames

In this section the first few mode shapes of the generic frames are presented in Table 4.6 - Table 4.10 and Figure 4.2 – Figure 4.6 below.

Table 4.6: First 5 mode shapes of the 6-storey frame.

Storey	Mode				
	1	2	3	4	5
1	0,1787	-0,4036	0,7659	-0,7992	0,9806
2	0,3546	-0,7027	0,9640	-0,3906	-0,4308
3	0,5248	-0,7531	0,2244	0,7607	-0,7007
4	0,6891	-0,5098	-0,8215	0,5618	1,0000
5	0,8472	0,0800	-1,0000	-1,0000	-0,5460
6	1,0000	1,0000	0,8168	0,3422	0,1188

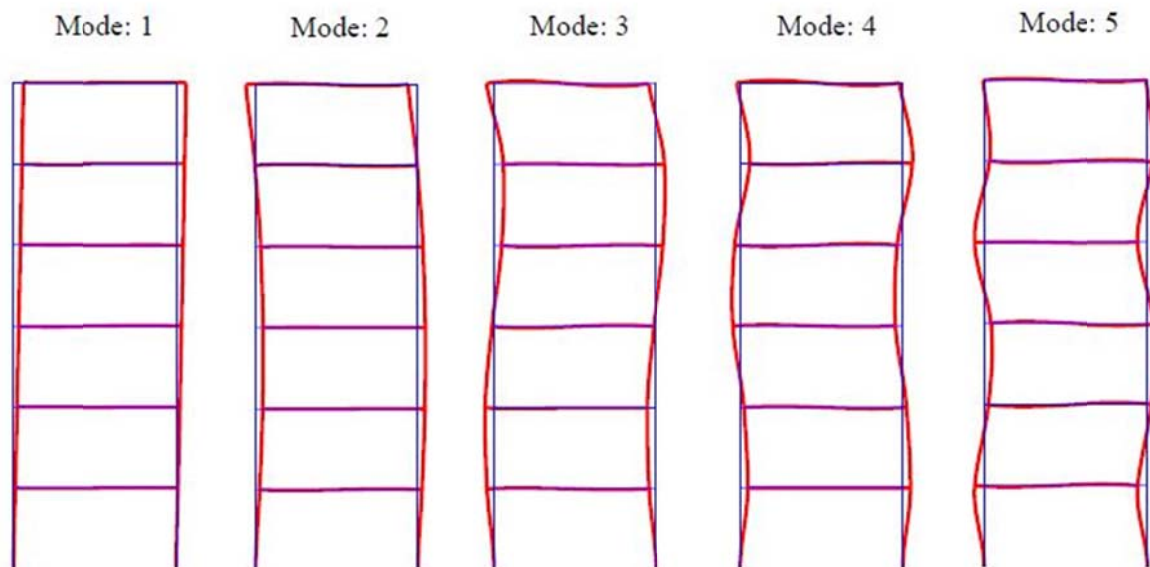


Figure 4.2: First five mode shapes of the six storey frame.

Table 4.7: First 5 mode shapes of the 9-storey frame.

Storey	Mode				
	1	2	3	4	5
1	0,1247	-0,2538	-0,5031	0,6584	0,7155
2	0,2481	-0,4751	-0,8301	0,8573	0,5894
3	0,3680	-0,6184	-0,7881	0,3177	-0,3630
4	0,4842	-0,6660	-0,4086	-0,5010	-0,8595
5	0,5960	-0,5939	0,1866	-0,9051	-0,1221
6	0,7034	-0,3923	0,7422	-0,4605	0,8517
7	0,8062	-0,0554	0,9270	0,5614	0,4103
8	0,9049	0,4134	0,4154	1,0000	-1,0000
9	1,0000	1,0000	-1,0000	-0,6633	0,3623

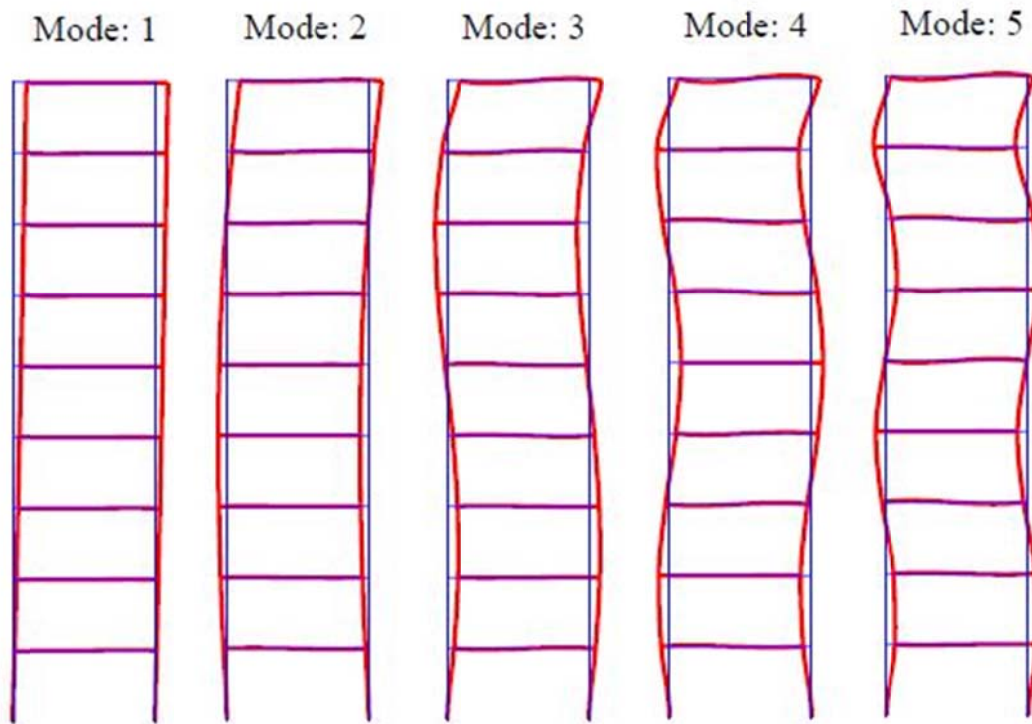


Figure 4.3: First five mode shapes of the nine storey frame.

Table 4.8: First 5 mode shapes of the 12-storey frame.

Storey	Mode				
	1	2	3	4	5
1	0,0967	-0,1880	0,3368	-0,5663	0,6094
2	0,1927	-0,3614	0,6038	-0,9017	0,8018
3	0,2868	-0,4989	0,7127	-0,7800	0,3273
4	0,3786	-0,5917	0,6498	-0,2899	-0,4082
5	0,4675	-0,6272	0,4167	0,3541	-0,8196
6	0,5532	-0,5992	0,0638	0,8389	-0,5591
7	0,6357	-0,5027	-0,3271	0,8911	0,2064
8	0,7148	-0,3357	-0,6487	0,4241	0,8228
9	0,7906	-0,0982	-0,7801	-0,3709	0,6273
10	0,8633	0,2074	-0,6029	-1,0000	-0,3624
11	0,9329	0,5764	-0,0219	-0,7683	-1,0000
12	1,0000	1,0000	1,0000	0,9358	0,5702

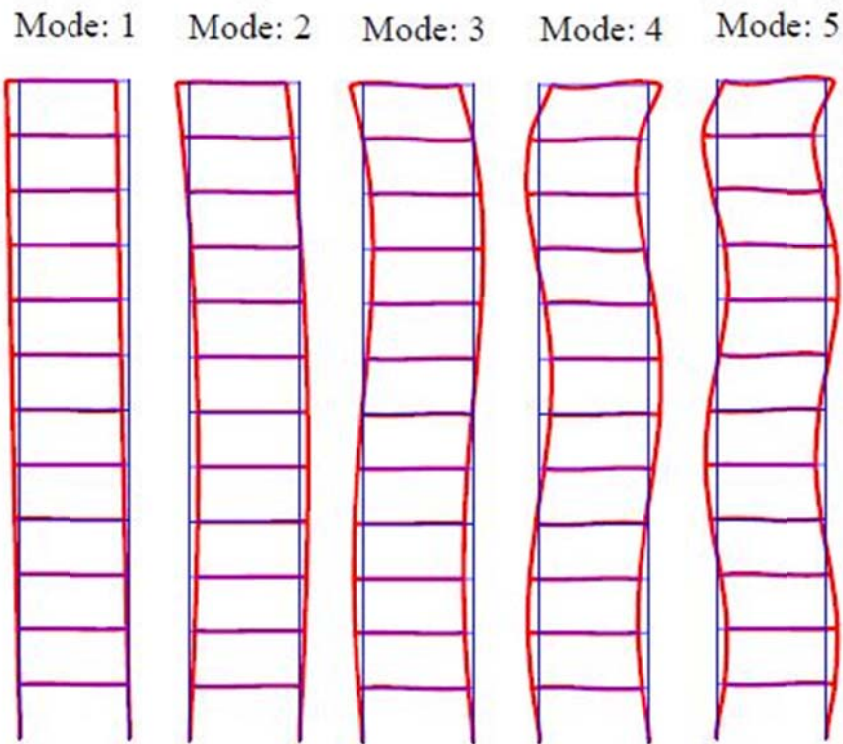


Figure 4.4: First five mode shapes of the nine storey frame.

Table 4.9: First 5 mode shapes of the 15-storey frame.

Storey	Mode				
	1	2	3	4	5
1	0,0775	0,1476	0,2479	-0,4213	0,5892
2	0,1548	0,2876	0,4624	-0,7319	0,9190
3	0,2311	0,4088	0,5980	-0,8011	0,7492
4	0,3062	0,5061	0,6410	-0,6287	0,2032
5	0,3797	0,5720	0,5784	-0,2547	-0,4533
6	0,4513	0,6024	0,4186	0,2074	-0,8823
7	0,5209	0,5932	0,1821	0,6126	-0,8410
8	0,5883	0,5421	-0,0966	0,8222	-0,3254
9	0,6535	0,4476	-0,3722	0,7439	0,4054
10	0,7165	0,3091	-0,5918	0,3702	0,9225
11	0,7773	0,1271	-0,6985	-0,1966	0,8412
12	0,8359	-0,0975	-0,6352	-0,7379	0,0913
13	0,8925	-0,3626	-0,3506	-0,9378	-0,8616
14	0,9471	-0,6652	0,1923	-0,4443	-1,0000
15	1,0000	-1,0000	1,0000	1,0000	0,8365

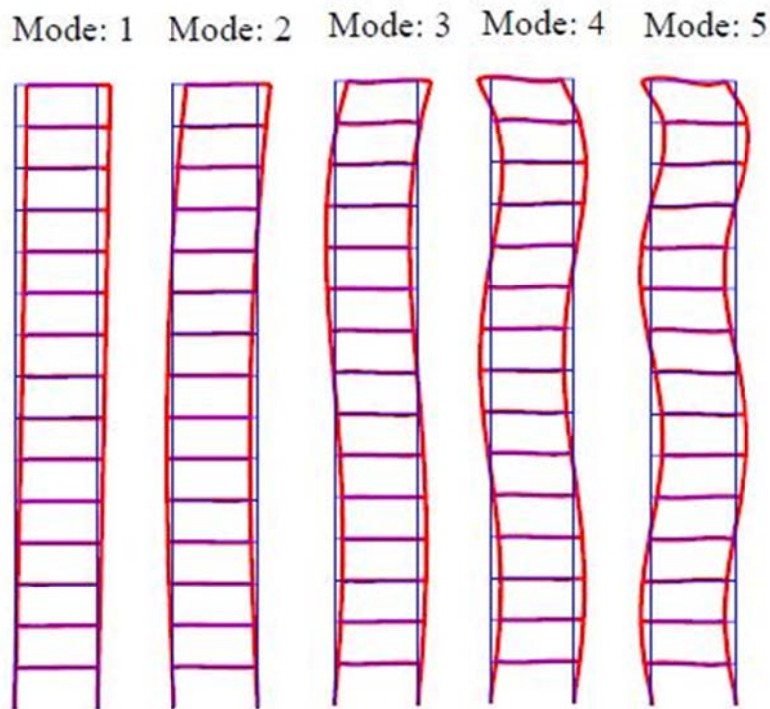


Figure 4.5: First five mode shapes of the fifteenth storey frame.

Table 4.10: First 5 mode shapes of the 18-storey frame.

Storey	Mode				
	1	2	3	4	5
1	-0,0641	-0,1210	0,1938	-0,3160	0,4756
2	-0,1281	-0,2376	0,3693	-0,5744	0,8065
3	-0,1917	-0,3432	0,5007	-0,7006	0,8309
4	-0,2547	-0,4347	0,5782	-0,6805	0,5672
5	-0,3168	-0,5075	0,5899	-0,5108	0,0965
6	-0,3778	-0,5586	0,5346	-0,2274	-0,4140
7	-0,4376	-0,5851	0,4158	0,1114	-0,7785
8	-0,4960	-0,5849	0,2446	0,4319	-0,8569
9	-0,5530	-0,5566	0,0379	0,6596	-0,6046
10	-0,6085	-0,4990	-0,1821	0,7337	-0,0999
11	-0,6626	-0,4116	-0,3890	0,6213	0,4695
12	-0,7151	-0,2942	-0,5533	0,3296	0,8594
13	-0,7661	-0,1470	-0,6436	-0,0854	0,8573
14	-0,8157	0,0293	-0,6282	-0,5158	0,3894
15	-0,8638	0,2339	-0,4769	-0,8055	-0,3807
16	-0,9104	0,4655	-0,1636	-0,7647	-1,0000
17	-0,9558	0,7219	0,3291	-0,2032	-0,7811
18	-1,0000	1,0000	1,0000	1,0000	0,9348

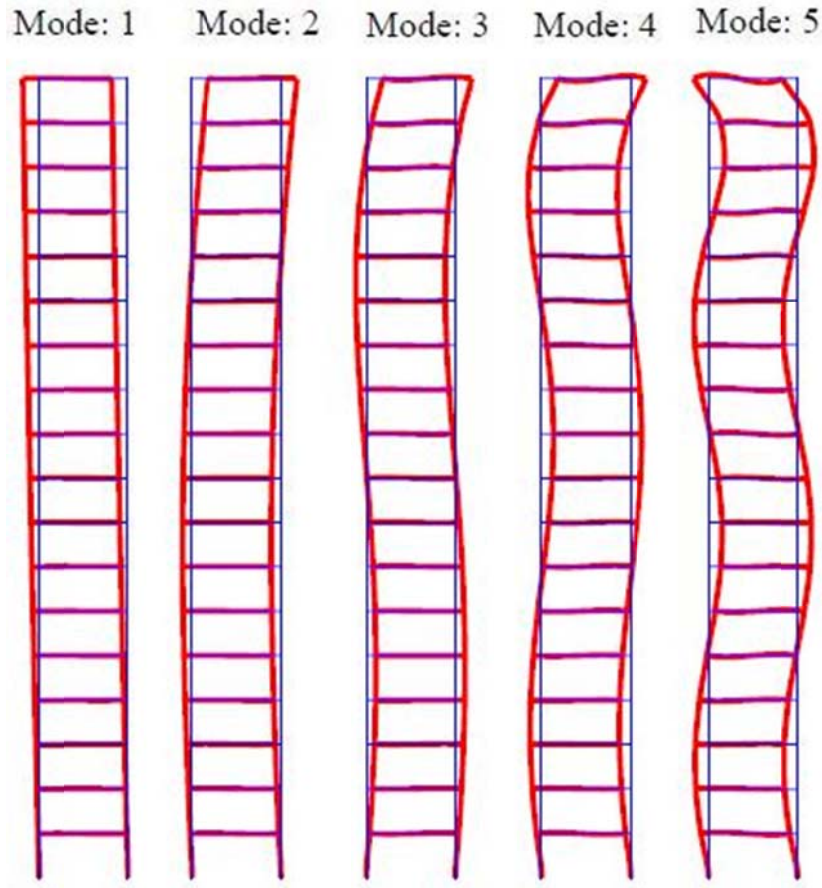


Figure 4.6: First five mode shapes of the eighteenth storey frame.

4.4 Modal analysis

This section describes briefly the method of modal analysis used in this study. Model analysis decouples the coupled system of differential equations of forced vibration into a set of N independent differential equations. The equation of forced vibration can be written in the matrix form as

$$[M]\{\ddot{u}\} + [C]\{\dot{u}\} + [K]\{u\} = \{p\} \quad ; \quad \{u(t = 0)\} = \{u_0\} \quad ; \quad \{\dot{u}(t = 0)\} = \{\dot{u}_0\} \quad (6)$$

where $\{p\} = -[M]\{r\}\ddot{u}_g$ is the dynamic load vector. $\{r\}$ is the influence vector which represents a rigid body motion of a structure. The influence vector for the frame structures studied herein has 1 in all the DOFs which correspond to the same motion component as the applied support motion, and 0 at other degrees of freedom. \ddot{u}_g is the ground acceleration due to earthquake motion.

The displacements, velocities and accelerations in Equation 6 are expressed in terms of their generalized coordinates resulting in

$$[M][\Phi]\{\ddot{y}\} + [C][\Phi]\{\dot{y}\} + [K][\Phi]\{y\} = \{p\} \quad (7)$$

where $[\Phi]$ is the mode shape matrix. Pre-multiplying both sides of Equation 7 with $[\Phi]^T$ gives

$$[\Phi]^T[M][\Phi]\{\ddot{y}\} + [\Phi]^T[C][\Phi]\{\dot{y}\} + [\Phi]^T[K][\Phi]\{y\} = [\Phi]^T\{p\} \quad (8)$$

Equation 8 can be written in terms of generalized mass, generalized damping and generalized stiffness matrices as

$$[\tilde{M}]\{\ddot{y}\} + [\tilde{C}]\{\dot{y}\} + [\tilde{K}]\{y\} = \{\tilde{p}\} \quad (9)$$

Where $\{\tilde{p}\} = [\Phi]^T\{p\}$ is a $N \times 1$ vector function of time known as generalized force vector. Its i^{th} row produces the generalized force of mode, \tilde{p}_i which is a function of time. The diagonal nature of the generalized matrices in Equation 9 suggests that the system is decoupled into N second order differential equations, the i^{th} one of which can be written as

$$\tilde{M}_i\ddot{y}_i + \tilde{C}_i\dot{y}_i + \tilde{K}_iy_i = \tilde{p}_i \quad (10)$$

This differential equation is in generalized coordinates y_i and its solution requires specification of initial conditions in the generalized coordinates as well. One way of finding the initial conditions is using the modal expansion of the displacement vector

$$\{u\} = \{\varphi_1\}y_1 + \{\varphi_2\}y_2 + \cdots \{\varphi_i\}y_i + \cdots \{\varphi_N\}y_N \quad (11)$$

Pre-multiplying Equation 11 with $\{\varphi_i\}^T[M]$ gives

$$\begin{aligned} \{\varphi_i\}^T[M]\{u\} &= \{\varphi_i\}^T[M]\{\varphi_1\}y_1 + \{\varphi_i\}^T[M]\{\varphi_2\}y_2 + \cdots \{\varphi_i\}^T[M]\{\varphi_i\}y_i \\ &\quad + \cdots \{\varphi_i\}^T[M]\{\varphi_N\}y_N \end{aligned} \quad (12)$$

where the orthogonal property of the mode shapes implies that all the terms on the right hand side except for $\{\varphi_i\}^T[M]\{\varphi_i\}y_i$ cancel out, thus giving

$$\{\varphi_i\}^T[M]\{u\} = \{\varphi_i\}^T[M]\{\varphi_i\}y_i \quad (13)$$

$$\Rightarrow y_i = \frac{\{\varphi_i\}^T[M]\{u\}}{\tilde{M}_i} \quad (14)$$

This equation provides the transformation of the structural coordinates to the generalized coordinates. Applying this at the initial time, gives us the initial conditions in in generalized coordinates, as

$$y_{0i} = \frac{\{\varphi_i\}^T [M] \{u_0\}}{\tilde{M}_i} \quad (15)$$

$$\dot{y}_{0i} = \frac{\{\varphi_i\}^T [M] \{\dot{u}_0\}}{\tilde{M}_i} \quad (16)$$

Then equations 10, 15 and 16 provide the differential equations, and associated initial conditions for the solution of generalized coordinates y_i of mode i . This set of equations is similar to that of forced vibration of a single degree of freedom (SDOF) system, and is solved in this project with the Newmark beta method. Once all the generalized coordinates $y_i, i = 1, 2, 3, \dots, N$ have been independently determined, the displacement of the structure can be found by transforming the generalized coordinates back into the geometrical coordinates, which is facilitated by the modal matrix as

$$\{u\} = [\Phi] \{y\} \quad (17)$$

This type of solution method, where the total response is found as a superposition of the response of individual modes of free vibration, is very useful in analysing linearly elastic systems (Rupakhety, 2011).

4.5 Time-history analysis and FEM solutions

In this study the Newmark's beta method is used in the time-history analysis with a time step equal to the time step of the recorded ground motion. Newmark beta method is a method of numerical integration used to solve differential equations developed by Nathan M. Newmark in 1959. The value used for beta in the time-history analysis is $\beta = 1/4$ which assumes that the acceleration is constant within a step and is therefore referred to as constant average acceleration method.

4.5.1 Computation of shear forces

With the displacement of the structure in global coordinates known the element forces can be solved. The element nodal displacement in local coordinates can be solved with

$$\{d_e\} = [T]\{D_e\} \quad (18)$$

where $[T]$ is the transformation matrix and $\{D_e\}$ is the element nodal displacement in global coordinates. The element end forces in local coordinates can be solved with

$$\{F_e\} = [K_e]\{d_e\} \quad (19)$$

where $\{F_e\}$ are the element end forces and $[K_e]$ is the elements stiffness matrix for a 2D frame element. For each element $\{F_e\}$ is a (6 x 1) vector where indexes 1 & 4 are the end normal forces. Indexes 2 & 5 are the end shear forces which are of interest in this study. Indexes 3 & 6 are the end moments.

4.5.2 Computation of storey forces

The equivalent lateral storey forces corresponding to the internal shear forces are of great interest in this study. The difference of shear forces between consecutive storeys gives the equivalent static storey forces at every storey. In this study the maximum absolute storey force for each storey through the time-history analysis is stored and this method is used for all the near-fault records for comparison and analysis. The maximum absolute of the storey forces is used because the frame structures will experience these forces during the time-histories though at different times. The storey forces are then normalized with the sum of the maximum absolute storey forces (base shear) to get a unit less result for further processing and comparison. An illustration of how to obtain storey forces is shown in Figure 4.7.

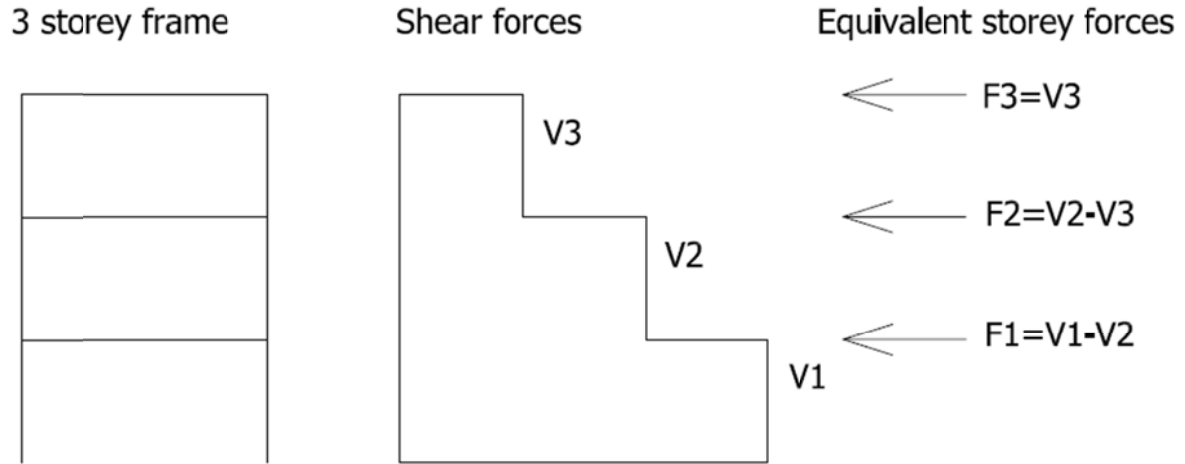


Figure 4.7: Illustration example of equivalent external storey forces (F_i) from shear forces (V_i). The sum of storey forces is equal to the base shear (V_1) referred to as F_b in EC8.

4.5.2.1 Eurocode 8 provisions

This section views the provisions of EC8 regarding approximating the horizontal storey forces due to ground motions. According to section 4.3.3.2.2. in EN 1998-1:2003 (Eurocode 8 : Design of structures for earthquake resistance -Part 1: General rules, seismic actions and rules for buildings).

(1) *The fundamental mode shapes in the horizontal directions of analysis of the building may be calculated using methods of structural dynamics or may be approximated by horizontal displacements increasing linearly along the height of the building.*

(2) *The seismic action effects shall be determined by applying, to the two planar models, horizontal forces F_i to all storeys.*

(3) *When the fundamental mode shape is approximated by horizontal displacements increasing linearly along the height, the horizontal forces F_i should be taken as being given by:*

$$F_i = F_b * \frac{z_i * m_i}{\sum z_j * m_j} \quad (20)$$

where

F_i is the horizontal force acting on storey i ;

F_b is the seismic base shear in accordance with expression;

z_i , z_j are the heights of the masses m_i , m_j above the level of application of the seismic action (foundation or top of a rigid basement).

(4)P The horizontal forces F_i determined in accordance with this clause shall be distributed to the lateral load resisting system assuming the floors are rigid in their plane.

F_b (Base shear) is the sum of F_i forces. For a structure with equal mass along height the slope of the function of F_i is constant.

5 Results and discussion

Figure 5.1 shows the velocity response spectra with 5% damping ratio of the 56 records in the dataset plotted in log-log scale along with the fundamental periods (T_1) of the frames.

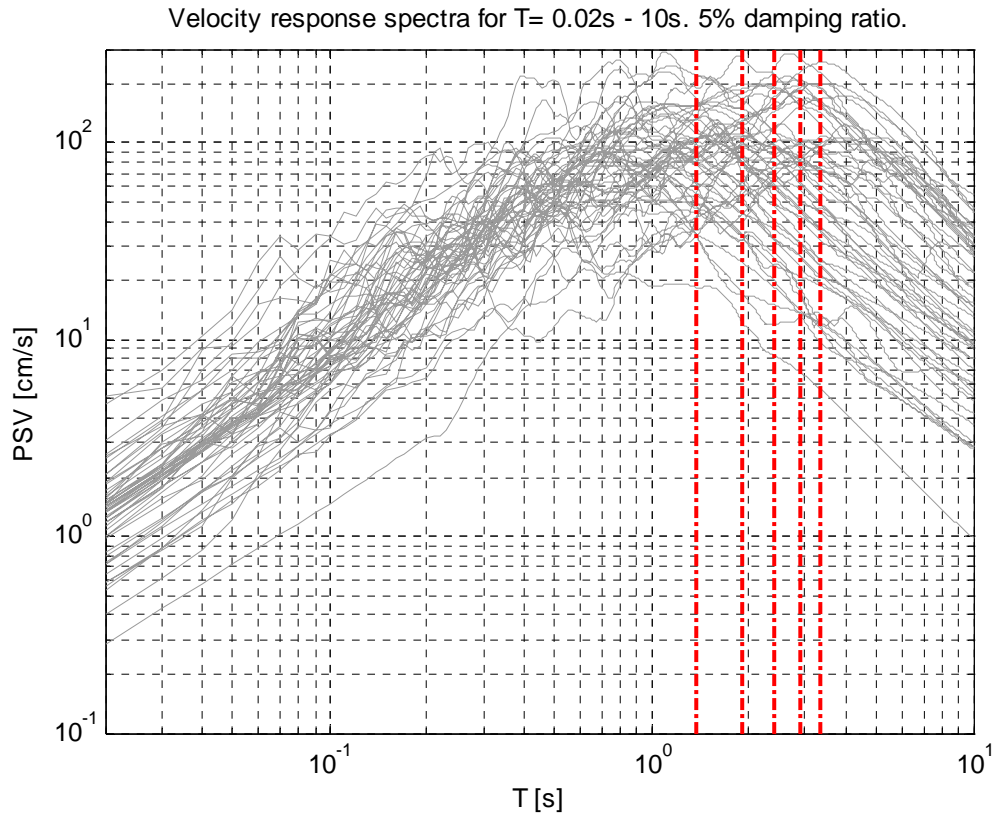


Figure 5.1: Velocity response spectra of the 56 records (log-log plot) are shown as grey lines. The fundamental periods of the frames are shown as the red dash dot lines (see fundamental periods of the frames in table 4.3).

Table 5.1 presents the mean maximum absolute storey forces and the base shear (F_b) which is the sum of the storey forces for each frame. Table 5.2 displays these values as a percentage of the base shear.

Table 5.1: Modelled mean maximum absolute storey forces for all the frames.

Mean Maximum absolute storey forces [kN]					
	Number of storeys				
	6	9	12	15	18
F1	33394	31274	30898	30537	30537
F2	40955	35131	32564	30757	30007
F3	44051	37816	34980	31415	29892
F4	47825	38792	36081	32484	29877
F5	53834	39728	36424	33749	29636
F6	75622	41599	37418	34168	30145
F7		42559	37047	33859	29993
F8		48581	37445	33532	29407
F9		72139	37867	34127	29637
F10			41025	33970	29746
F11			47020	34189	30306
F12			70414	36205	30822
F13				39199	31050
F14				44794	31888
F15				67872	33438
F16					35450
F17					41072
F18					63547
Fb	295680	387618	479183	550858	596450

Table 5.2: Modelled mean maximum absolute storey forces as percentage of base shear for all the frames.

Mean Maximum absolute storey forces [% of Fb]					
	Number of storeys				
	6	9	12	15	18
F1	11,3	8,1	6,4	5,5	5,1
F2	13,9	9,1	6,8	5,6	5,0
F3	14,9	9,8	7,3	5,7	5,0
F4	16,2	10,0	7,5	5,9	5,0
F5	18,2	10,2	7,6	6,1	5,0
F6	25,6	10,7	7,8	6,2	5,1
F7		11,0	7,7	6,1	5,0
F8		12,5	7,8	6,1	4,9
F9		18,6	7,9	6,2	5,0
F10			8,6	6,2	5,0
F11			9,8	6,2	5,1
F12			14,7	6,6	5,2
F13				7,1	5,2
F14				8,1	5,3
F15				12,3	5,6
F16					5,9
F17					6,9
F18					10,7
Fb	100,0	100,0	100,0	100,0	100,0

The maximum absolute normalized storey forces from the 56 records obtained from time-history analysis can be seen in figures Figure 5.2 - Figure 5.6 where the height of the structure is normalized with total height.

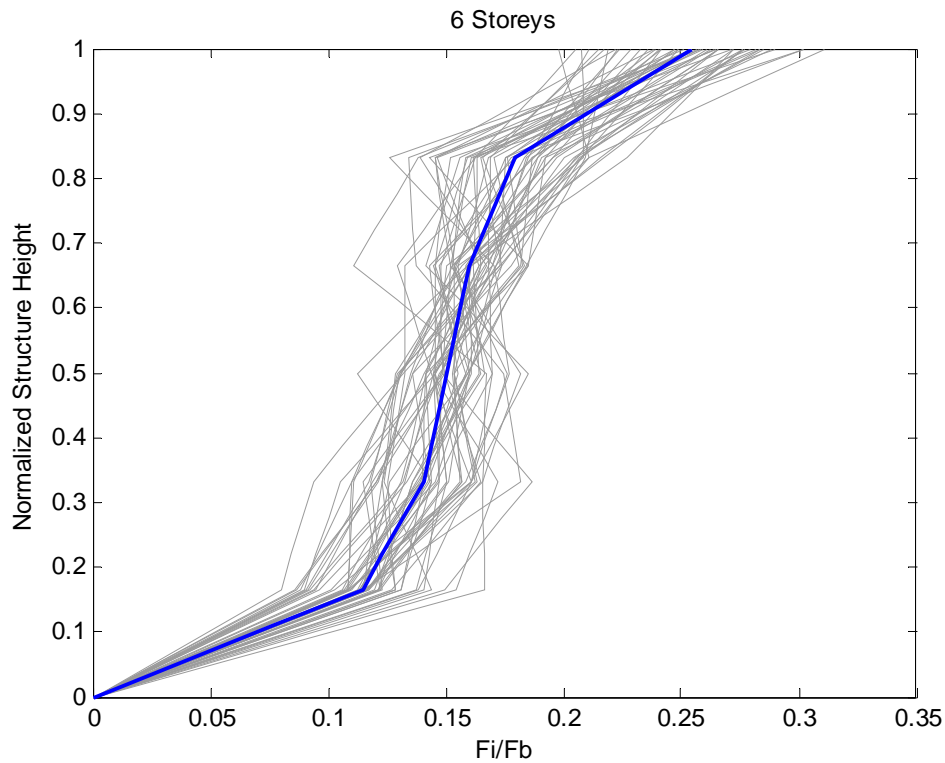


Figure 5.2: Plot of normalized storey forces along normalized height for the 6 storey frame structure. The absolute maximum of the 56 records are shown as grey lines. The mean values of the 56 records are shown as a blue line.

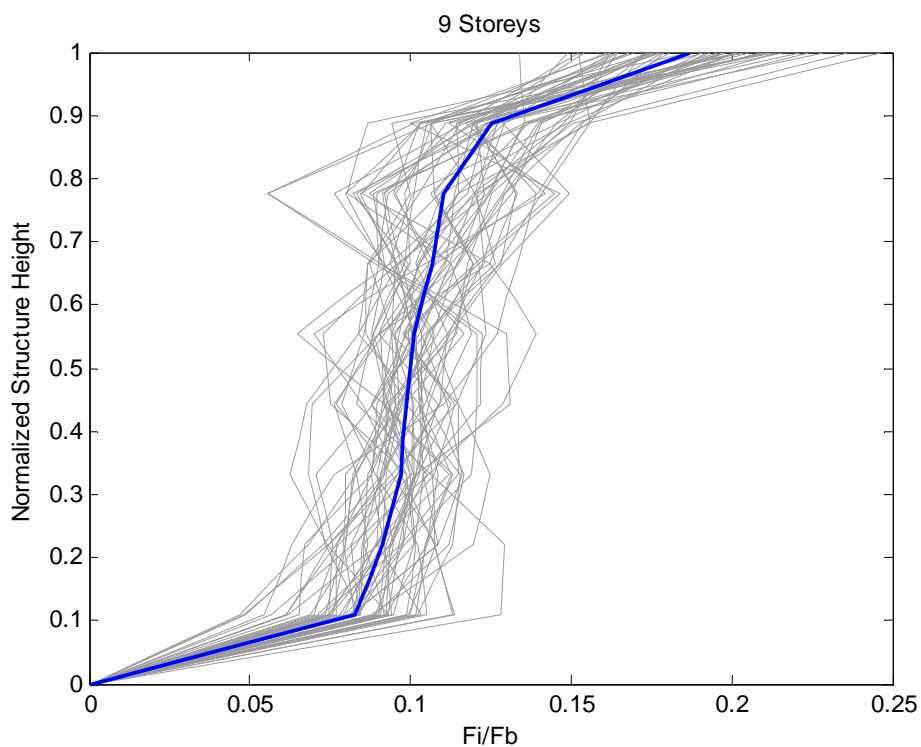


Figure 5.3: Plot of normalized storey forces along normalized height for the 9 storey frame structure. The absolute maximum of the 56 records are shown as grey lines. The mean values of the 56 records are shown as a blue line.

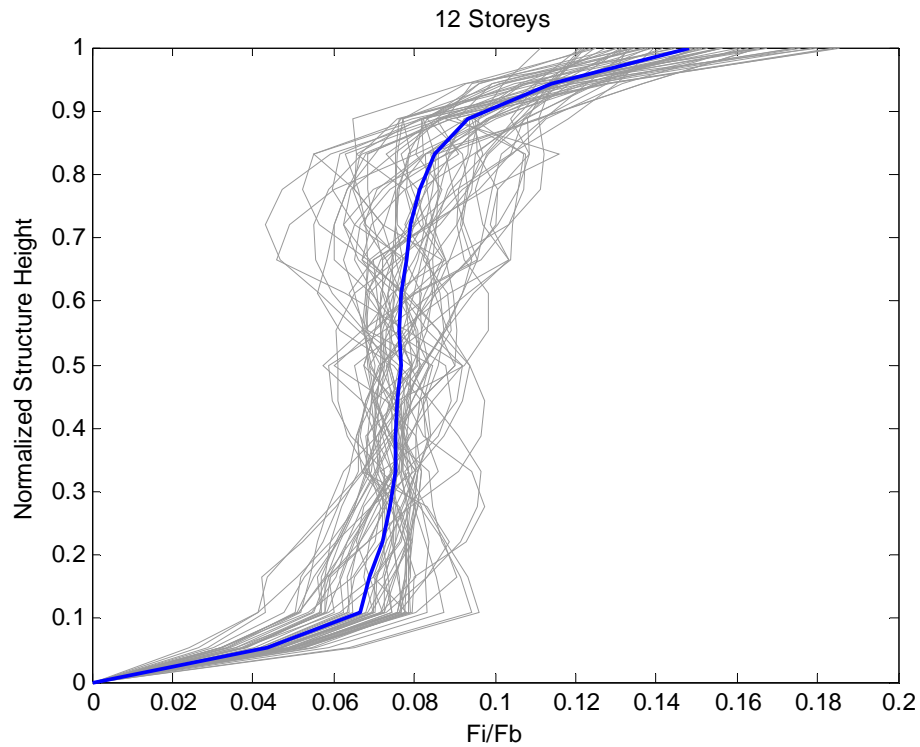


Figure 5.4: Plot of normalized storey forces along normalized height for the 12 storey frame structure. The absolute maximum of the 56 records are shown as grey lines. The mean values of the 56 records are shown as a blue line.

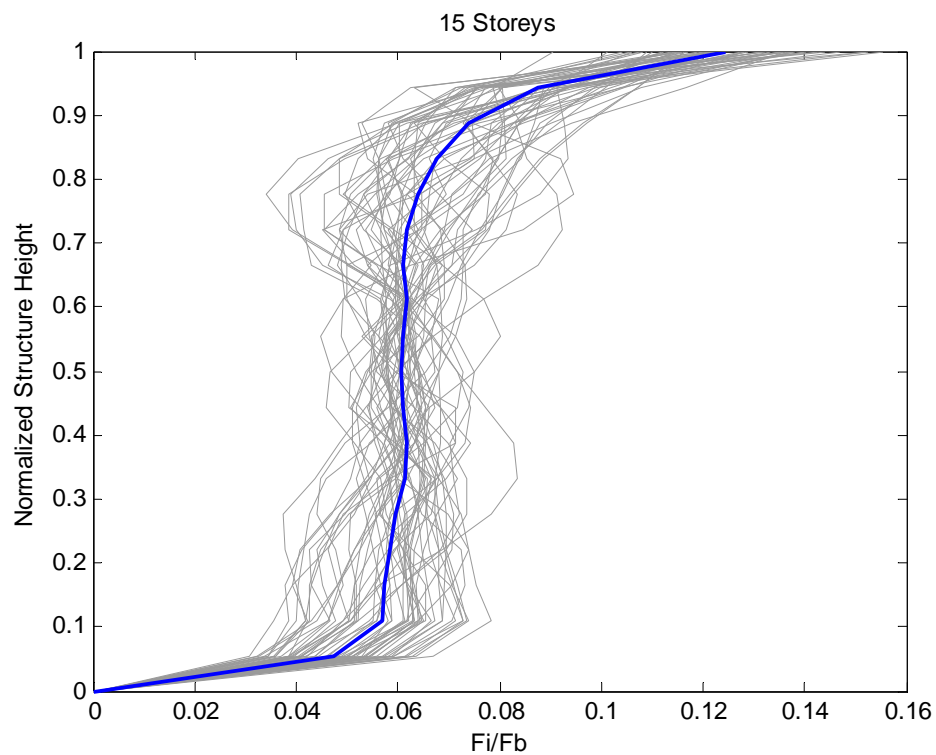


Figure 5.5: Plot of normalized storey forces along normalized height for the 15 storey frame structure. The absolute maximum of the 56 records are shown as grey lines. The mean values of the 56 records are shown as a blue line.

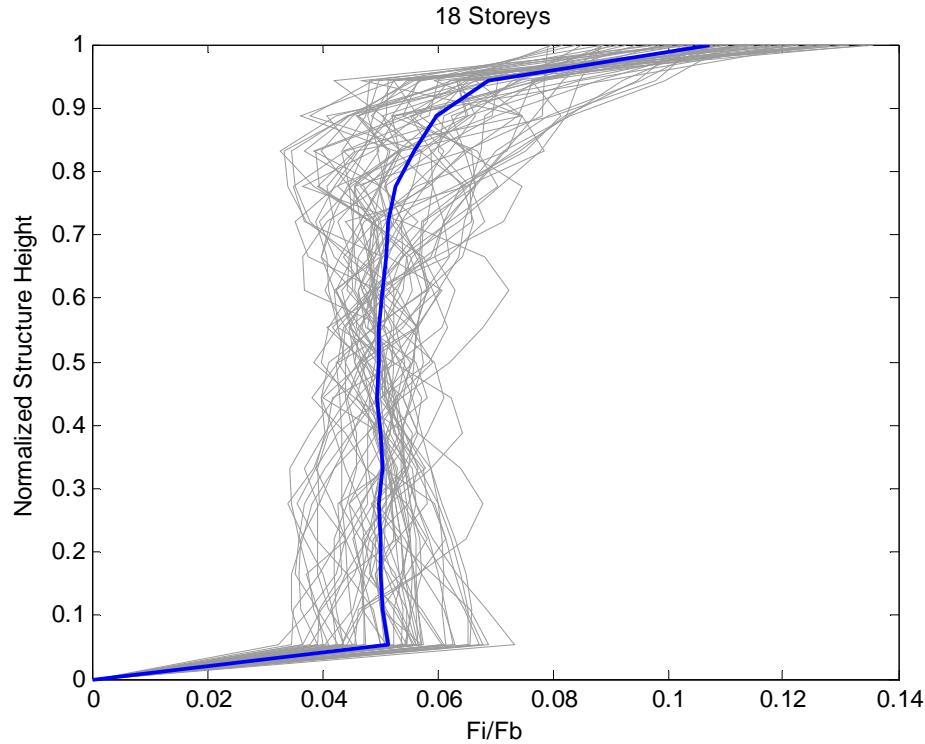


Figure 5.6: Plot of normalized storey forces along normalized height for the 18 storey frame structure. The absolute maximum of the 56 records are shown as grey lines. The mean values of the 56 records are shown as a blue line.

Figure 5.2 - Figure 5.6 show that the maximum absolute storey force distributions of the 56 records have similar patterns for each structure.

- The mean distribution of storey forces for the six storey frame resembles the first mode shape of a one bay frame structure. The response of the first mode shape of the frame is dominant but higher modes are also contributing to the response.
- The distributions of maximum absolute storey forces of the 9 storey frame shows that higher modes are contributing more to the response than for the 6 storey frame, because the distribution of storey forces for the 9 storey frame differs more from the linear distribution of the linear first mode shape.
- The distribution of storey forces of the 12 storey frame differs more from the 6 storey frame than the 9 storey frame.
- The distribution of storey forces of the 15 storey frame differs more from the 9 storey frame than the 12 storey frame.
- The storey forces for the eighteen storey frame have a very different distribution than the six storey frame. As the total height of the frames increases, the higher modes contribute more to the response. For the eighteenth storey structure the mean

distribution of storey forces is almost constant from near ground level to approximately 80% of the total height.

5.1 Model results compared with EC8 provisions

Majority of accelerograms are recorded far from causing ground motion fault, design codes are therefore dominated by provisions based on ground motions in the far-field region. The method in EC8 to find the equivalent static forces for MDOF systems approximates the dynamic behaviour by considering only a single mode (the first mode). It is therefore interesting to compare storey forces time-history analysis to EC8 provisions. Figure 5.7 shows the mean of maximum absolute storey forces normalized with the base shear for each of the frames. For comparison the distribution of normalized storey forces according to EC8 are also presented. The EC8 provision distributes the base shear linearly along the height of a structure, as the equivalent storey forces, to simulate the response of a structure to ground motion.

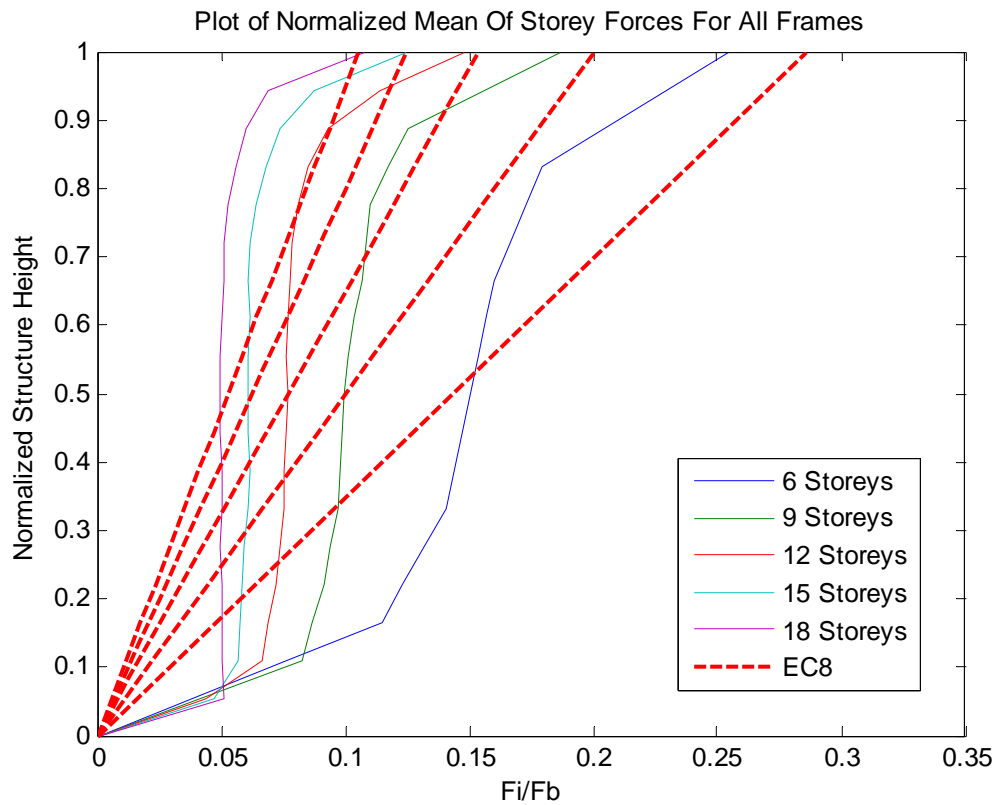


Figure 5.7: Mean values of normalized storey forces for all the frame structures compared with EC8 normalized provision for storey forces.

Figure 5.7 shows that the method in EC8 does not simulate the distribution of storey forces accurately based on the results from the time-history analysis. Again it should be mentioned that the storey forces in Figure 5.7 are normalized with the base shear. The storey forces

distribution for the six storey frame shows the closest resemblance to the EC8 storey force distribution. As the height of the frames increases, the difference between the modelled storey force distribution and the EC8 distribution increases. This suggest that for near-fault sites EC8 might not satisfy the possible storey forces for the lower half of tall structures but for the upper half of structures the provision is excessive based on these results. This means that in a strong near-fault ground motion a structure might experience excessive non-linear behaviour in the lower half of its total height but remain linear-elastic in the upper half of its total height if it were designed by considering only a single mode for horizontal storey forces as is described by Equation 20, which is taken from EC8. In Figure 5.8 below the mean of time-history storey force distribution for the frames are normalized with the force at the roof.

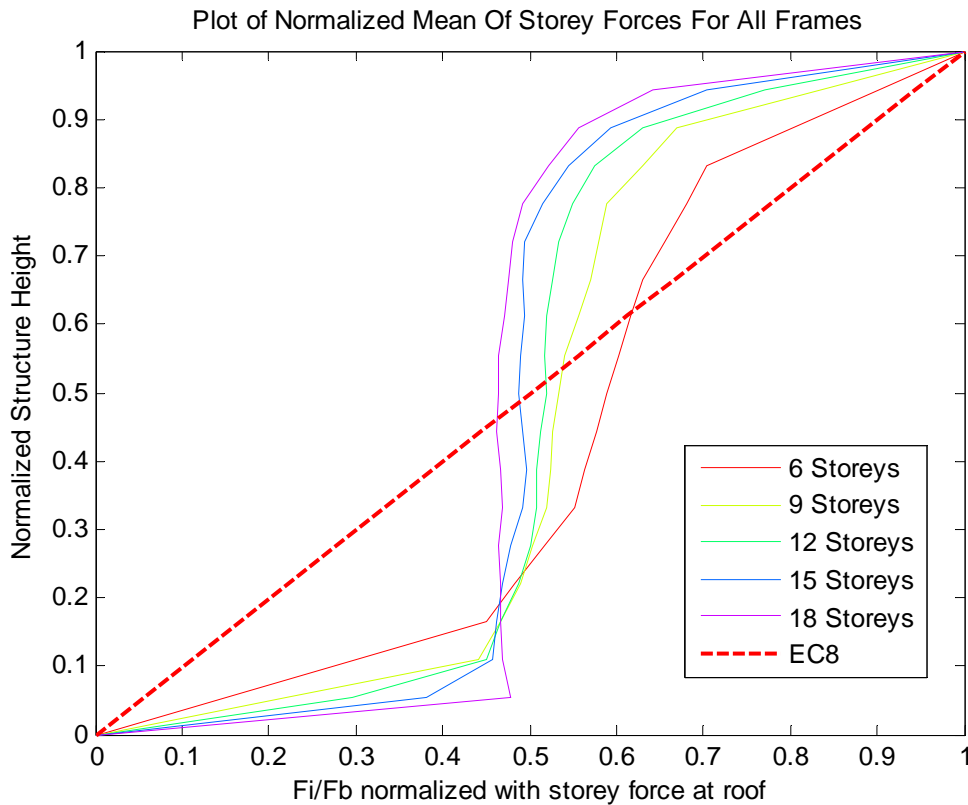


Figure 5.8: Mean values of normalized storey forces for all six frames, normalized with the storey force at roof, compared with EC8 normalized provision for storey forces.

The results in Figure 5.8 show how the time history storey force distribution results differ increasingly from the EC8 storey force provision as the total height of the frame increases from ground level to near 15% of relative height. At relative height between near 15% and around 45-60% of the frames the opposite occurs where the results differ decreasingly from the EC8 storey force provision as the height of the frame increases. At relative height near

45-60% of the frames the modelled time history force distributions cross the EC8 storey force provision. Above relative height around 45-60% until approaching the top, the time history storey force distribution results differ increasingly from the EC8 storey force provision as the total height of the frame increases. At the top the modelled storey force distributions of the frames gets close to the EC8 storey force provision. This again implies that the EC8 provision for equivalent storey forces might not simulate adequately linear-elastic response for structures due to near-fault ground motion.

Figure 5.9 shows the mean, of all structures, storey force which shows higher demand in the lower half and lower demand in the upper half of the structures when compared to the EC8 provision. The mean force distribution shown in Figure 5.9 might be a reasonable design model to replace the EC8 model.

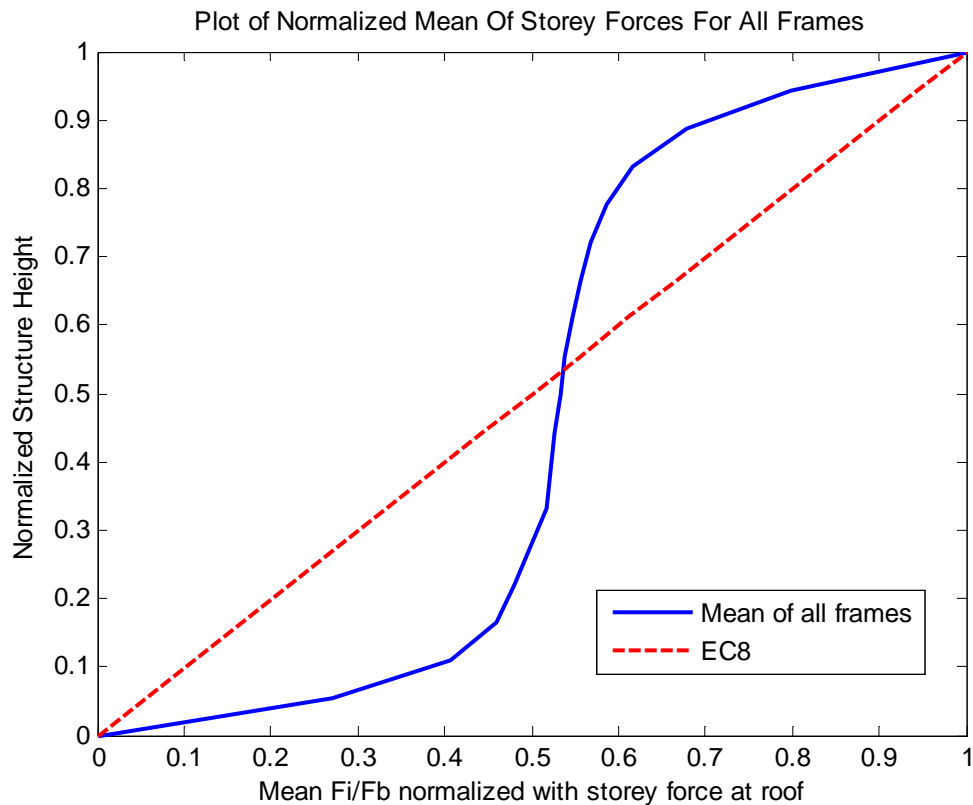


Figure 5.9: Mean for all the frames in one curve compared with EC8 provision for storey forces.

5.1.1 Difference of storey force results and EC8 provisions due to predominant period

It is of interest to analyse the difference in response of the frame structures due to the dominant period (T_d) of the earthquakes in the dataset. Structures with fundamental periods close to the predominant period of ground motion are expected to be affected more severely than others. It is therefore important to estimate the period where structures are most seriously impacted. The predominant period T_d is defined by Rupakhety *et al.* (2010) as the period where 5% damped linear-elastic-pseudo-velocity spectra reaches its peak value (see T_d values for the records in Table 9.1 in Appendix). If more than one peak of comparable amplitudes exists then the longest period is considered. The relationship between earthquake magnitude and the predominant period can be obtained without the time-history according to Rupakhety *et al.* (2010).

$$\log(T_d) = -3.09 + 0.51M_w \quad (21)$$

The normalized pulse period is $T_n = \frac{T_1}{T_d}$ where T_1 is the fundamental period of each structure and T_d is the dominant pulse period of the earthquakes. The fundamental periods of the frame structures are shown in Table 5.3:

Table 5.3: Fundamental periods of the frames

Mode(n)	Modal vibration period T_n (sec)				
	Number of storeys				
	6	9	12	15	18
1	1,379	1,910	2,411	2,892	3,362

The normalized periods from the dataset used are sorted into three groups for each frame:

$$0.7 \leq T_n < 1.3$$

$$1.3 \leq T_n < 2.0$$

$$2.0 \leq T_n$$

Table 5.4: Number of records in each T_n group for each frame

Group	No. Of records in each group for each frame				
	Storey height				
	6	9	12	15	18
$0.7 \leq T_n \leq 1.3$	21	18	18	19	16
$1.3 \leq T_n < 1.3$	11	12	14	14	9
$2.0 \leq T_n$	3	12	18	22	31
Σ	35	42	50	55	56

Figure 5.10 - Figure 5.14 show the mean distribution of storey forces for each group of normalized periods along with the maximum absolute storey force distribution of the 56 records and the EC8 storey force distribution.

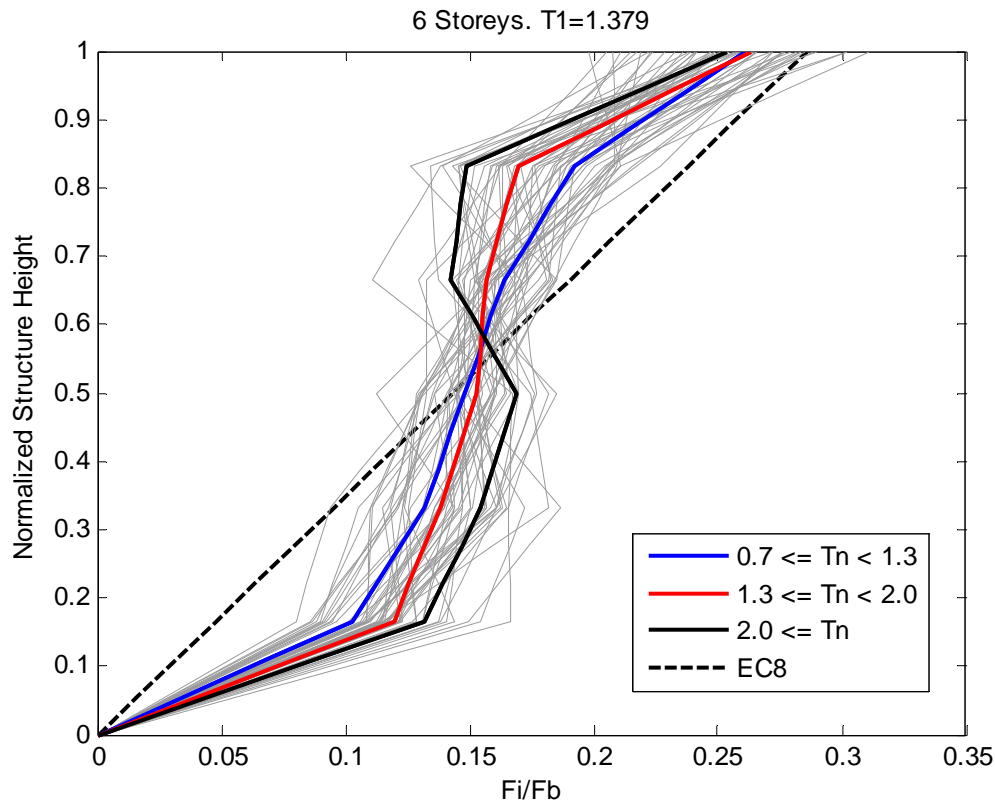


Figure 5.10: Mean storey forces for each normalized period group plotted with all maximum absolute storey forces and EC8 storey force distribution for the 6 storey frame.

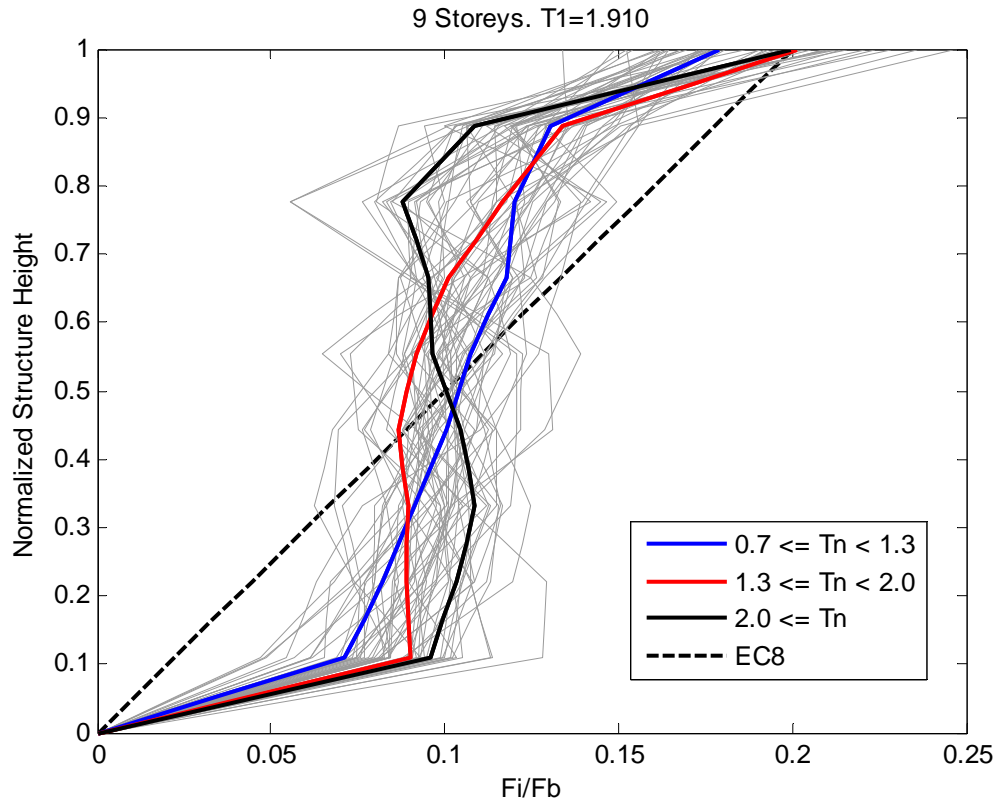


Figure 5.11: Mean storey forces for each normalized period group plotted with all maximum absolute storey forces and EC8 storey force distribution for the 9 storey frame.

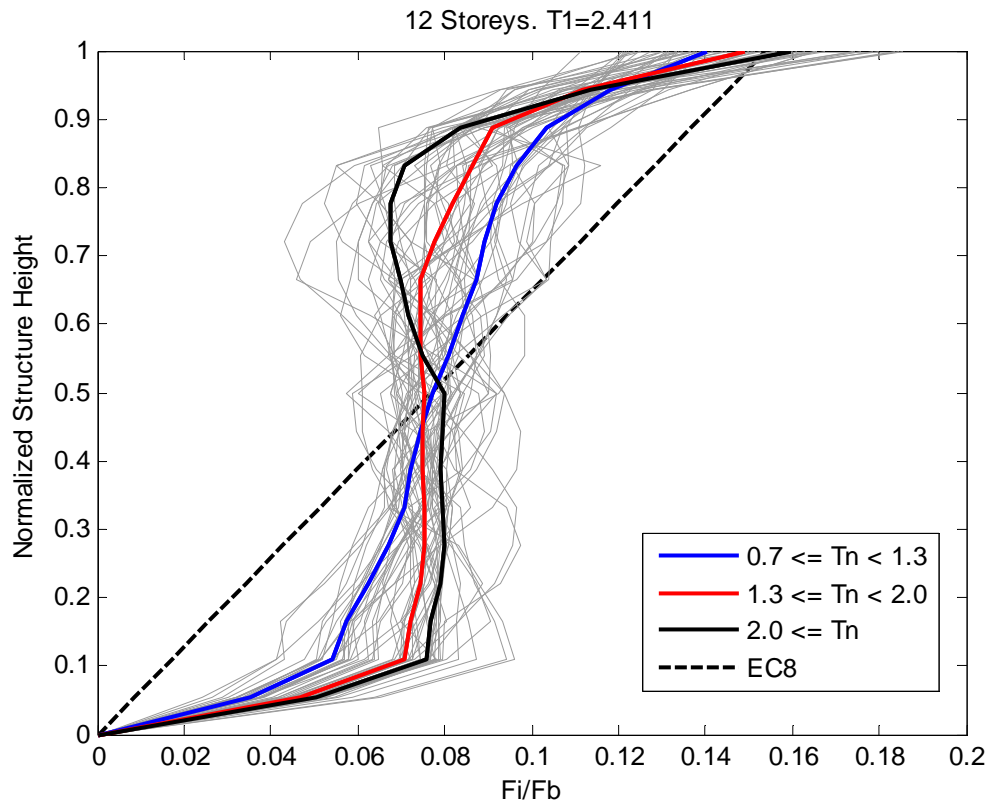


Figure 5.12: Mean storey forces for each normalized period group plotted with all maximum absolute storey forces and EC8 storey force distribution for the 12 storey frame.

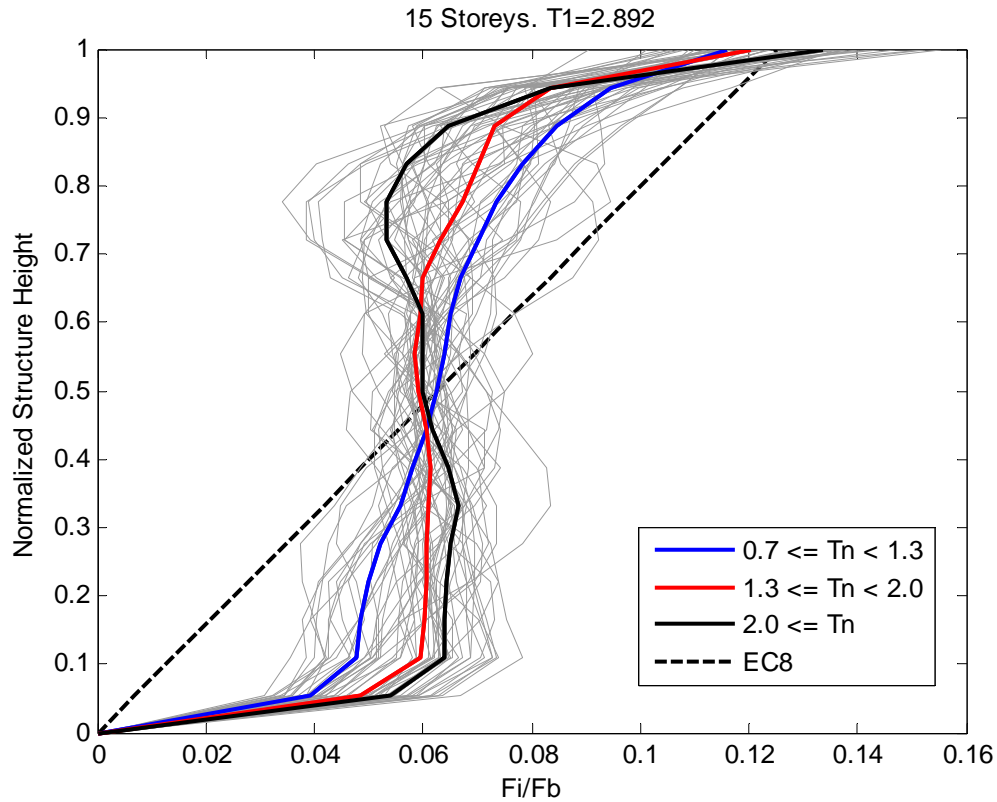


Figure 5.13: Mean storey forces for each normalized period group plotted with all maximum absolute storey forces and EC8 storey force distribution for the 15 storey frame.

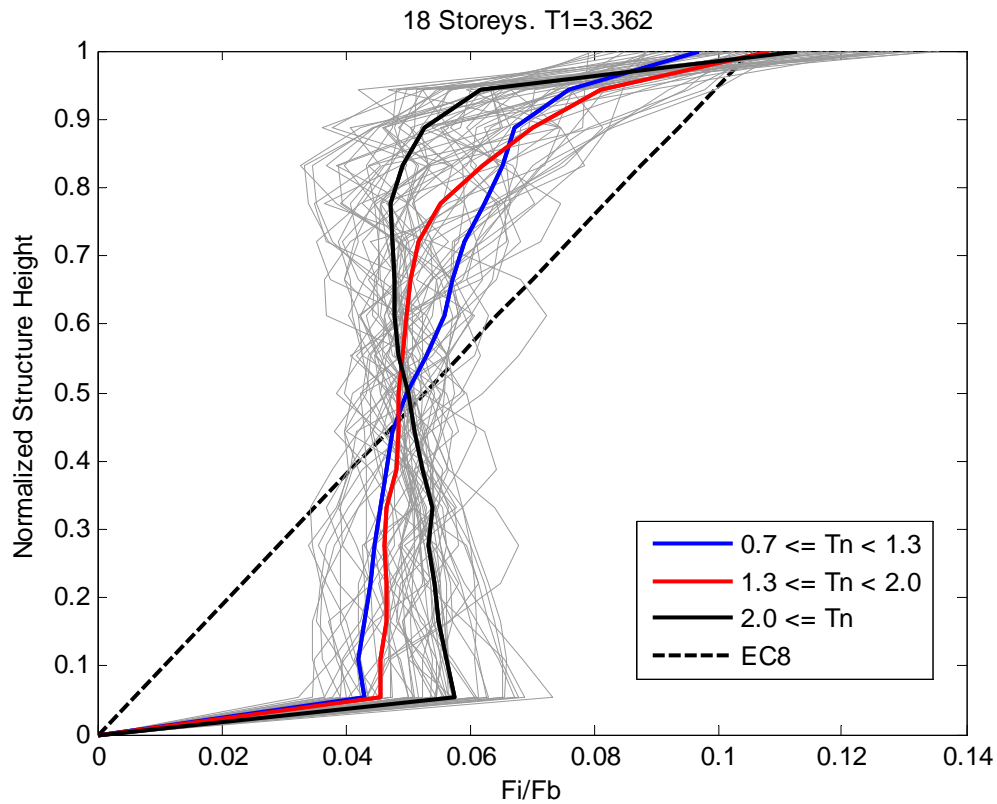


Figure 5.14: Mean storey forces for each normalized period group plotted with all maximum absolute storey forces and EC8 storey force distribution for the 18 storey frame.

Figure 5.10 - Figure 5.14 show how the predominant pulse period (T_d) affects the distribution of the storey forces. The general pattern is that as the normalized period is higher, results deviate more from the EC8 provisions. This means that when the predominant pulse period (T_d) is shorter than the fundamental period (T_1) of the frame, the storey force distribution deviates significantly from the EC8 provisions. This is not surprising because for ground motions where the predominant pulse period is shorter than the fundamental period of a structure, the predominant pulse period is exciting the higher modes more than the fundamental mode. When the normalized period is less than 1, the higher modes are excited by lower amplitude components of ground motion, and consequently, higher mode effects are suppressed resulting in a force distribution which is caused by the fundamental mode.

Looking at the normalized periods in groups it is easy to see the difference in response due to the fundamental period of the structures. The difference between the computed and EC8 storey force distribution is plotted in Figure 5.15 - Figure 5.19.

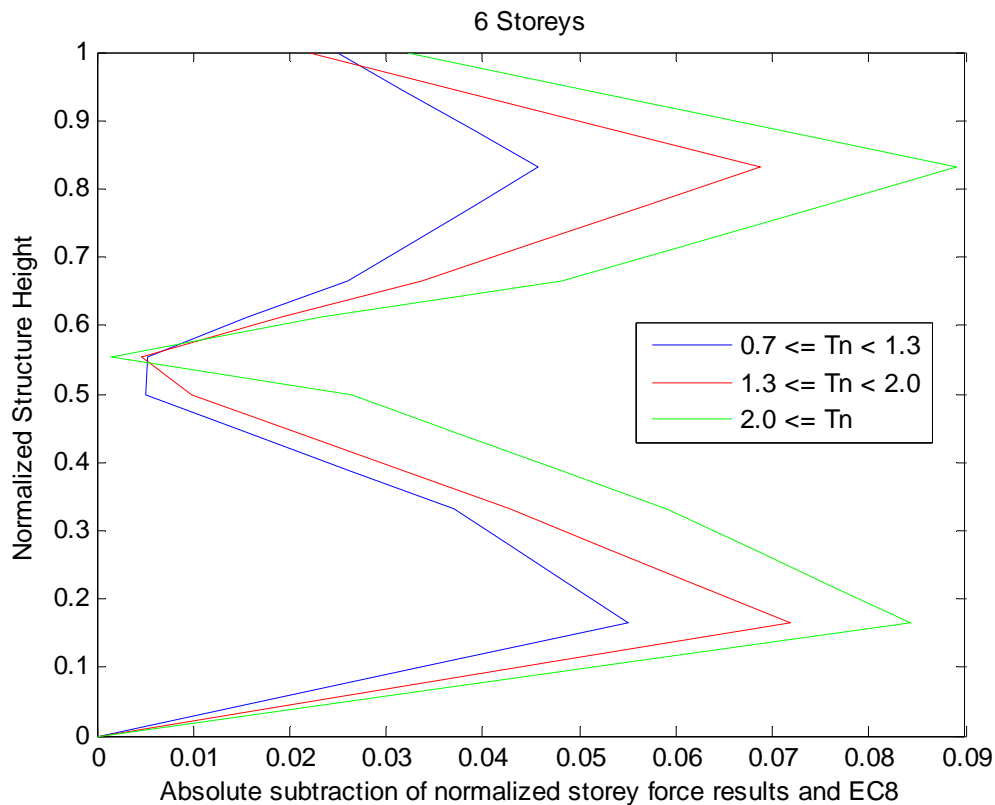


Figure 5.15: Plot of the mean difference of absolute normalized storey forces between near-fault modelling and normalized EC8 provisions for a 6 storey structure.

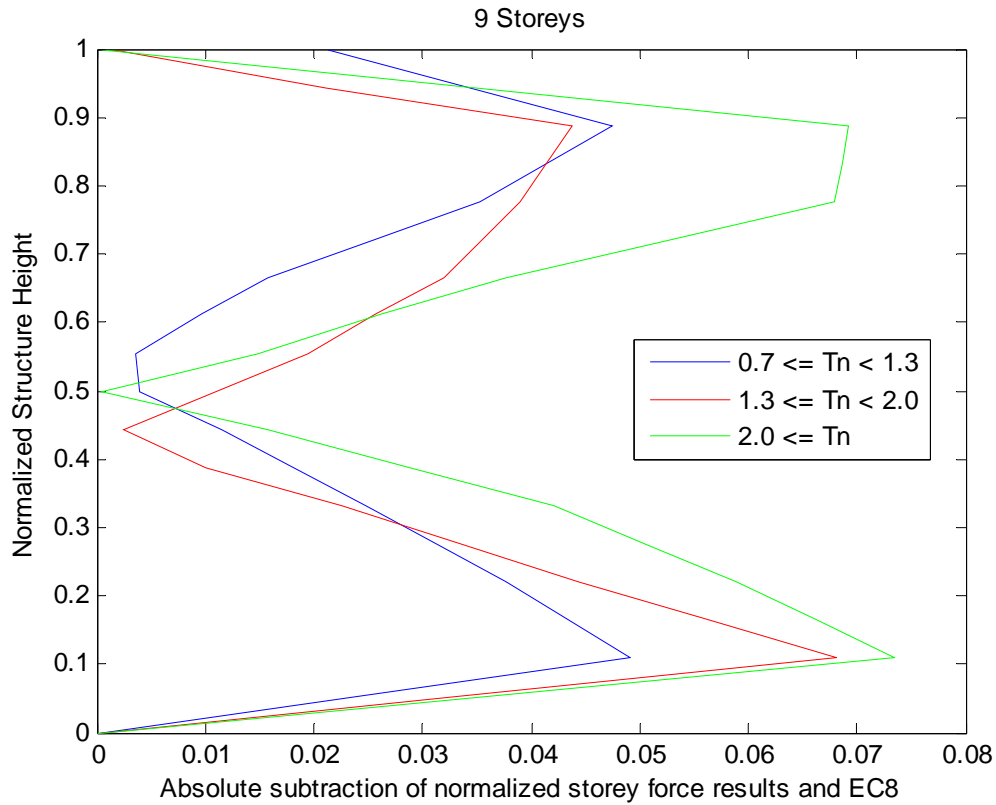


Figure 5.16: Plot of the mean difference of absolute normalized storey forces between near-fault modelling and normalized EC8 provisions for a 9 storey structure.

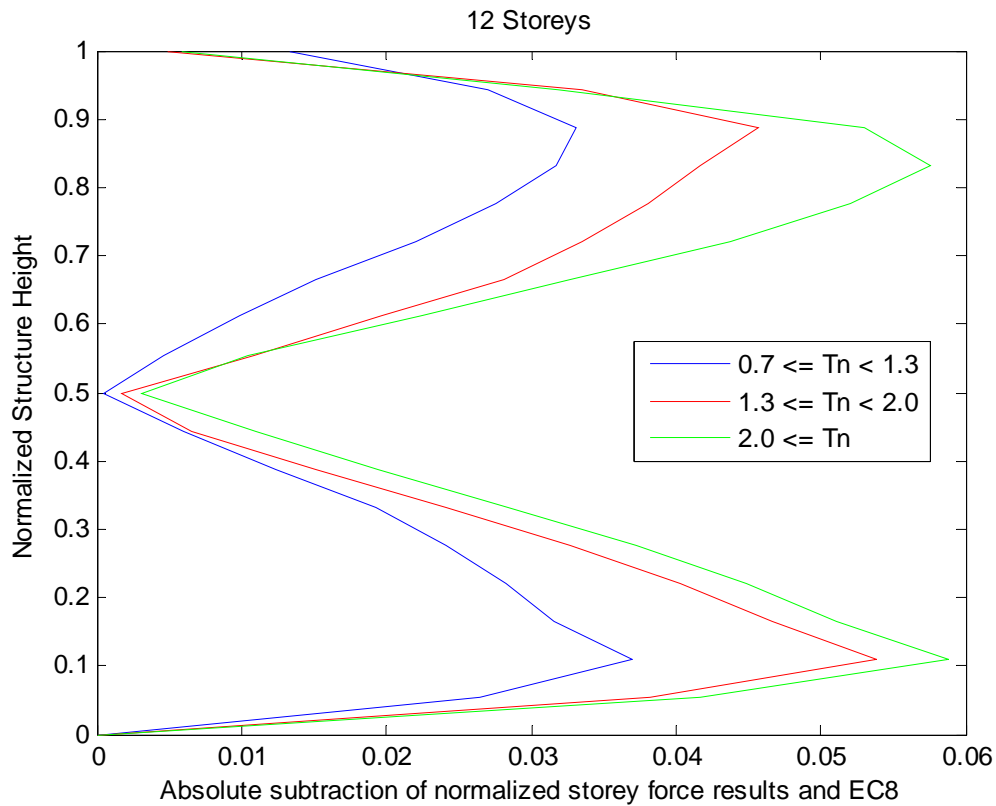


Figure 5.17: Plot of the mean difference of absolute normalized storey forces between near-fault modelling and normalized EC8 provisions for a 12 storey structure.

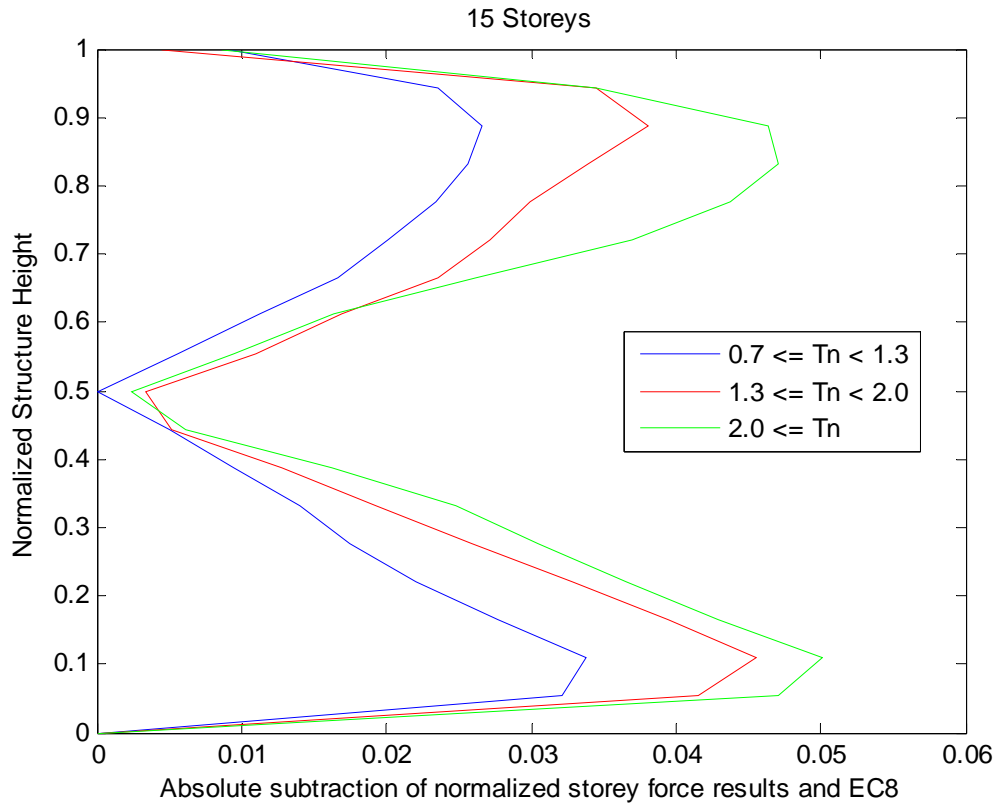


Figure 5.18: Plot of the mean difference of absolute normalized storey forces between near-fault modelling and normalized EC8 provisions for a 15 storey structure.

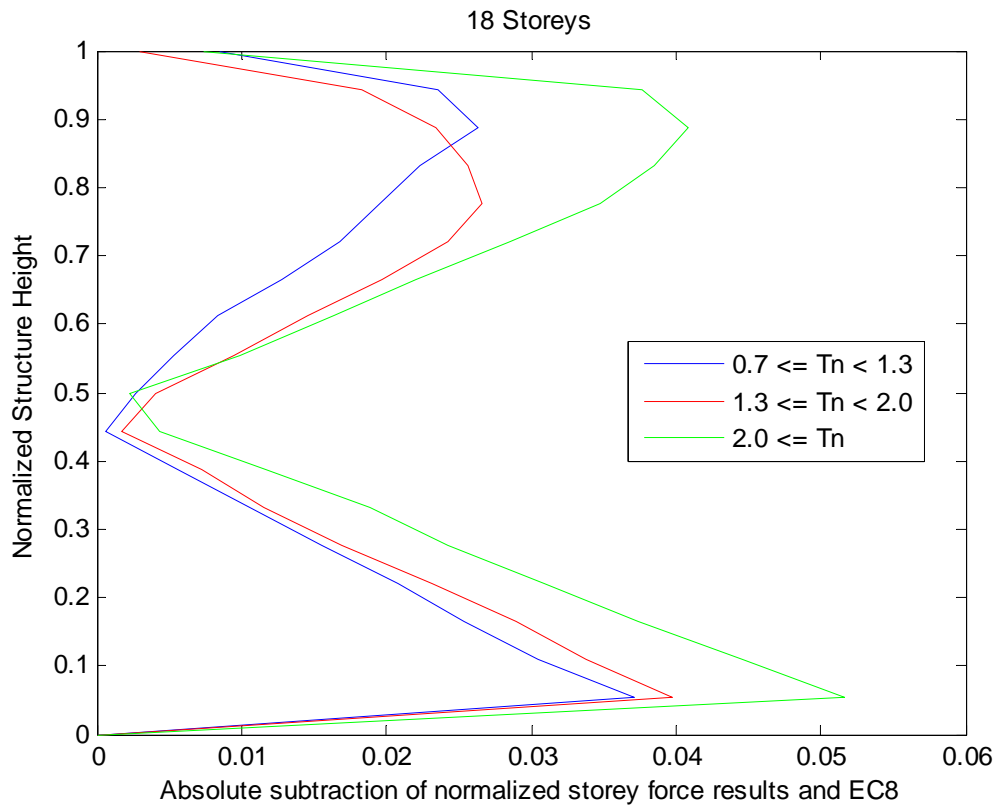


Figure 5.19: Plot of the mean difference of absolute normalized storey forces between near-fault modelling and normalized EC8 provisions for an 18 storey structure.

By looking at Figure 5.15 - Figure 5.19 it can be seen that the general pattern is that the difference between the storey force distribution results and the EC8 storey force distribution increases with higher T_n for all the frame structures. Figure 5.15 shows that the difference between the time-history results and EC8 is higher for the six storey frame than the other frames but the time history results were normalized with the sum of storey forces (base shear).

5.1.2 Difference of storey force results and EC8 provision at specific heights

Results in Figure 5.15 - Figure 5.19 displayed that the maximum difference between the storey force distribution results and EC8 storey force distribution was at height around 5-20% and 80-90% from ground but the difference at 50% of height was close to none where the curves of storey force results and the EC8 intersected.

Figure 5.20 - Figure 5.22 show the difference between the time-history results and EC8 provisions as a function of the normalized period (T_n) at relative heights 1/3, 2/3 and 3/3 from base of the frames.

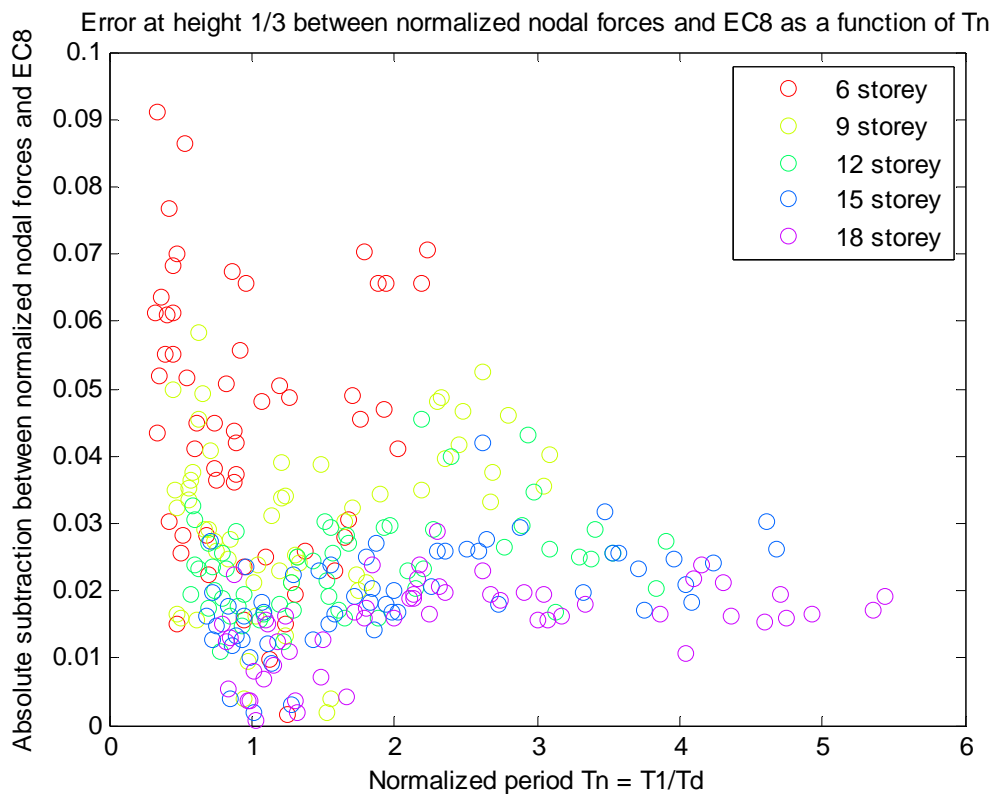


Figure 5.20: Difference of all near-fault ground motions storey forces and EC8 distribution as a function of normalized period T_n at height 1/3 of the 6,9,12,15 and 18 storey frames.

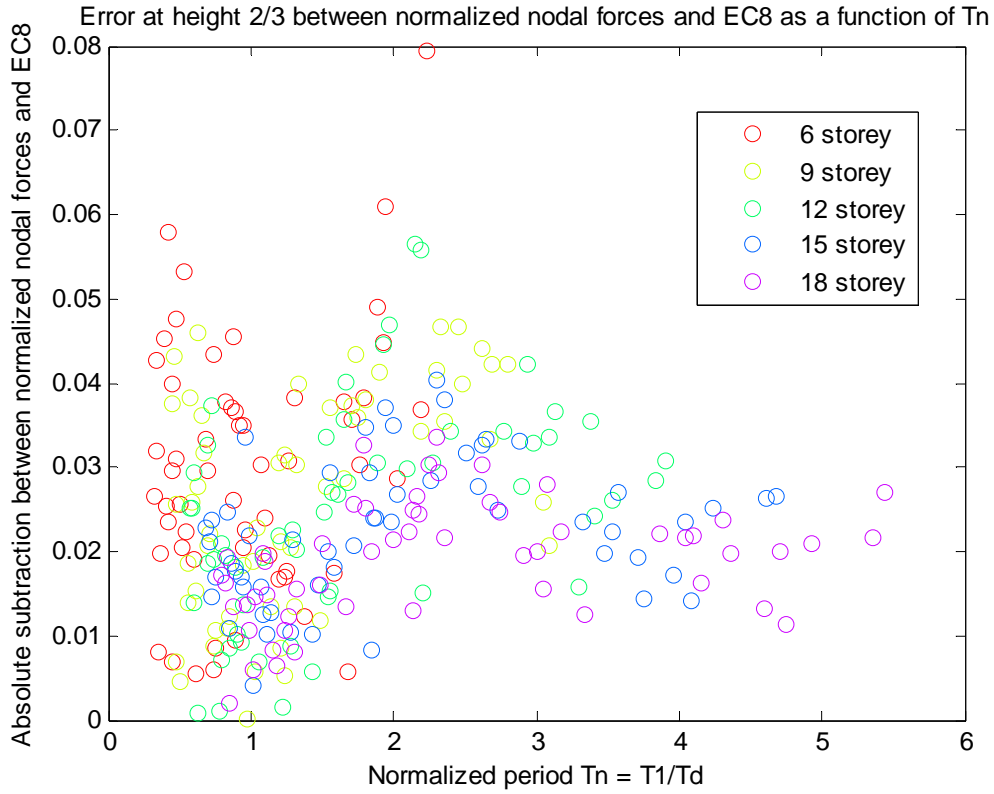


Figure 5.21: Difference of all near-fault ground motions storey forces and EC8 distribution as a function of normalized period T_n at height 2/3 of the 6,9,12,15 and 18 storey frames.

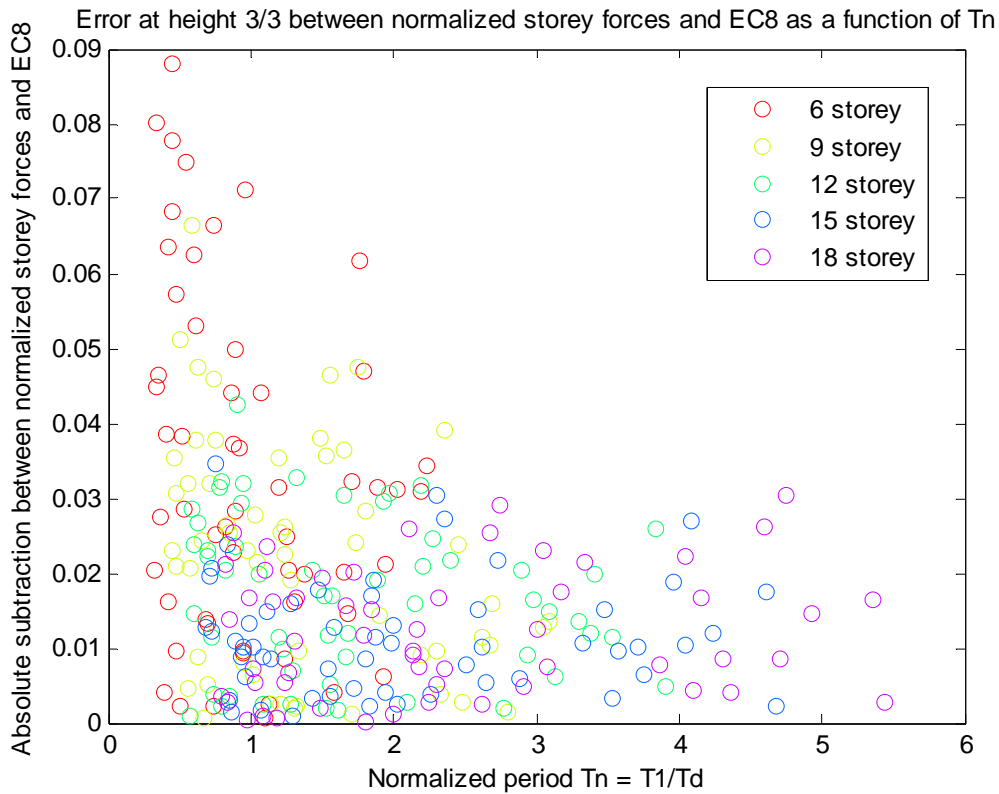


Figure 5.22: Difference of all near-fault ground motions storey forces and EC8 distribution as a function of normalized period T_n at height 3/3 of the 6,9,12,15 and 18 storey frames.

The pattern from Figure 5.20 - Figure 5.22 is questionable because the distribution of normalized storey forces is different for each frame and therefore the absolute subtraction between the storey forces for each frame and EC8 provision distribution are quite different at different heights. This makes comparison at specific heights between the frames non-relative. The values of the normalized period show though the distribution of normalized periods for each frame structure where the normalized periods for the six storey frame structure generally have the shortest normalized period and the taller frames reaching in the area where the longest normalized periods are.

6 A new model for storey force distribution in near-fault regions

The results give an opportunity to develop an improvement to the EC8 storey force distribution which is suitable for modelling static equivalent storey forces on structures in near-fault areas. The purpose is to propose a model that is relevant but simple. A function which simulates the equivalent lateral storey forces when fitted to the mean time history storey forces results in this study. Two models are presented. Model I is a fifth order polynomial with a very good fit to the mean storey force results. Model II is a third order polynomial which doesn't fit as well as model I but is simpler. The models are a continuous function of height of a structure where the relative height (h_i) gives the storey force at specific storey height. The storey forces are obtained with:

$$F_i = F_b * \left(\frac{g(h_i)}{\sum_{i=1}^{NS} g(h_i)} \right) \quad (22)$$

Where

$$h_i = \frac{H_i}{NS}$$

$$0 < h_i \leq 1$$

F_i is the horizontal force acting on storey i

F_b is the seismic base shear in accordance with expression

H_i is the storey number of structure

NS is the total number of storeys of structure

h_i is the relative height of structure

Model I:

$$g(h) = Ah^5 + Bh^4 + Ch^3 + Dh^2 + Eh \quad (23)$$

Where the constants are:

$$A = 21.237$$

$$B = -54.489$$

$$C = 53.769$$

$$D = -25.211$$

$$E = 1 - A - B - C - D = 5.694$$

Model II:

$$g(h) = Ah^3 + Bh^2 + Ch \quad (24)$$

Where the constants are:

$$A = 1.3\pi$$

$$B = -2\pi$$

$$C = 1 - A - B = 3.1991$$

The proposed models are plotted in Figure 6.1 and Figure 6.2 where h (relative height) is plotted on y-axis and the function value $g(h)$ is plotted on x-axis.

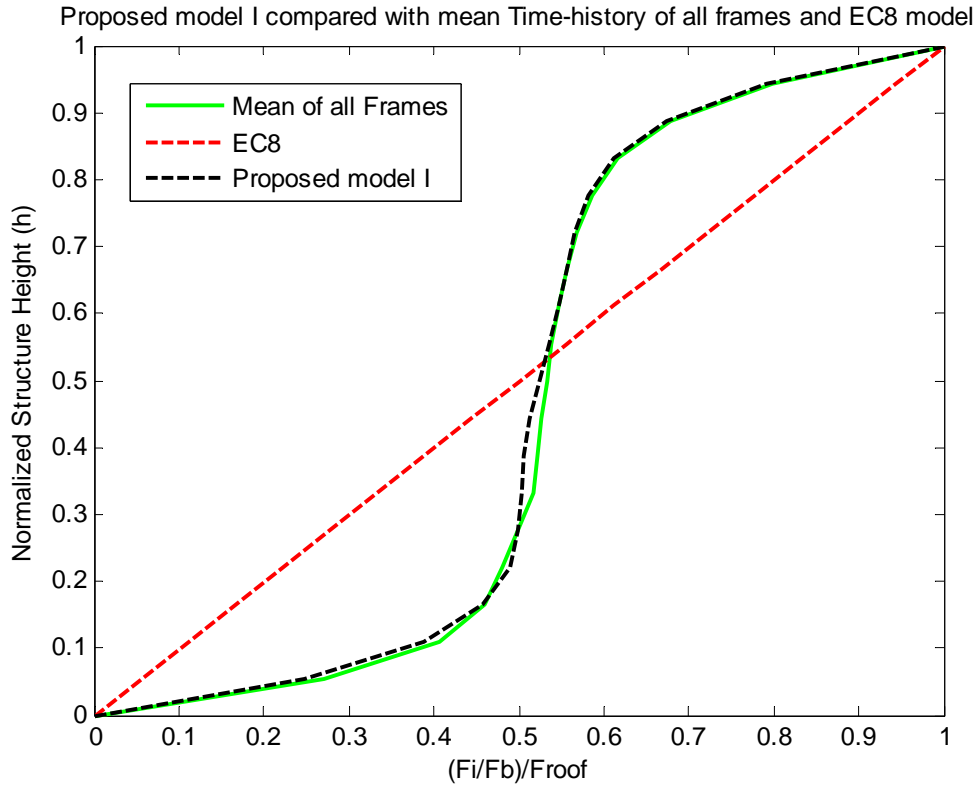


Figure 6.1: Proposed model I fitted to the mean time-history storey force results for all the frames and EC8 model.

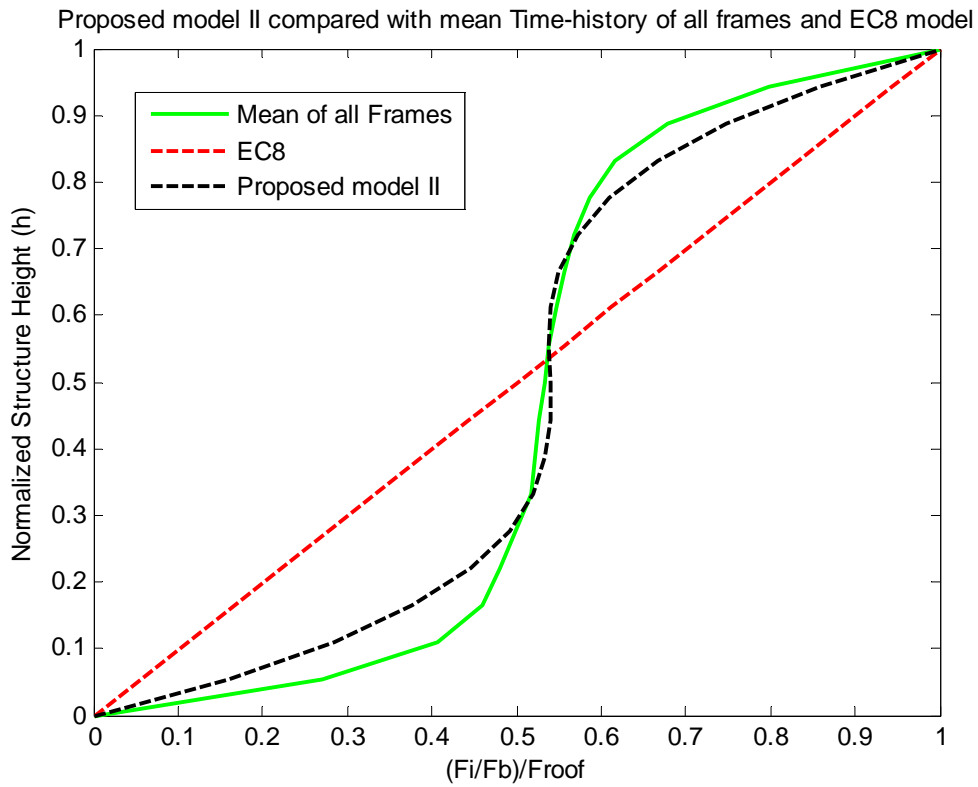


Figure 6.2: Proposed model II fitted to the mean time-history storey force results for all the frames and EC8 model.

These models are valid only in the near-fault area (within 20-25km from the fault) and only for events within the range of earthquake magnitudes considered in this study (5.0 to 6.93 in moment magnitude scale). Model II is selected for further analysis in this project due to its simplicity.

6.1.1 Effect of Normalized pulse period on mean time-history storey force response of frames

In Figure 6.3 - Figure 6.7 the proposed model II is compared with the mean time-history results for all the frames and the effects of T_n to the mean time-history force distribution are analysed.

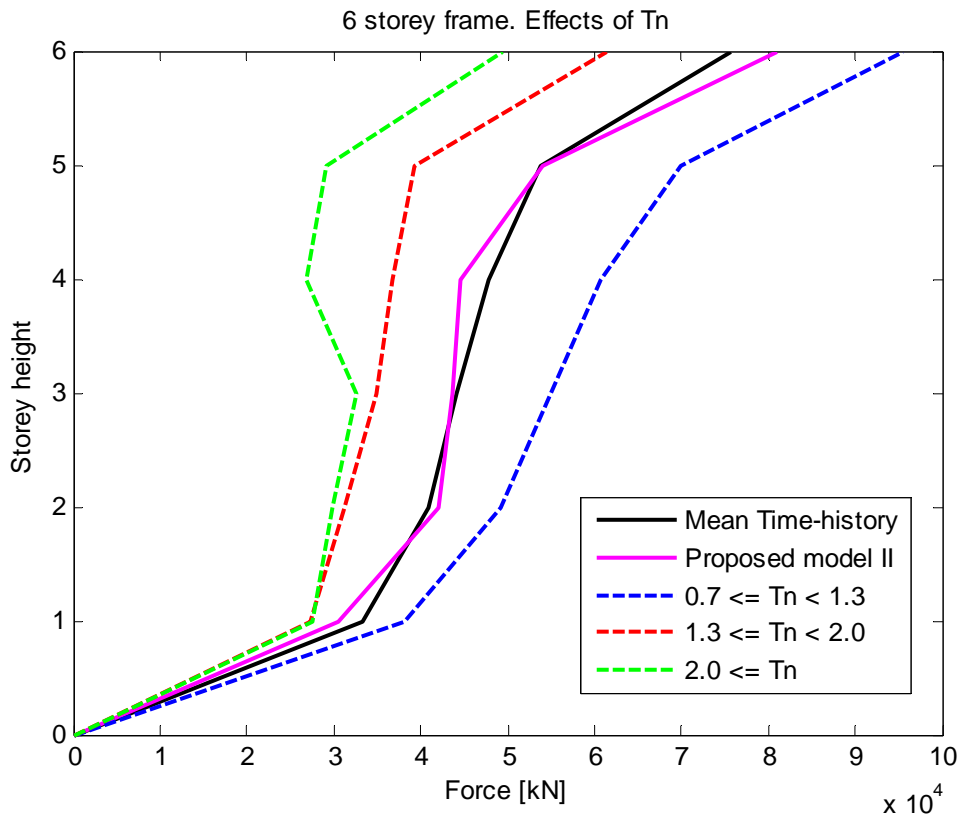


Figure 6.3: Proposed model II compared with the mean time-history results for the six storey frame. Effects of T_n groups to the storey force response shown along.

Figure 6.3 for the six storey frame shows that the ground motion series group of $0.7 \leq T_n < 1.3$ causes the highest force contribution to the mean time-history storey force response because in this group the predominant pulse period is close to the fundamental period of the frame which has the highest effective modal mass. The proposed model fits the mean time-history quite well in Figure 6.3.

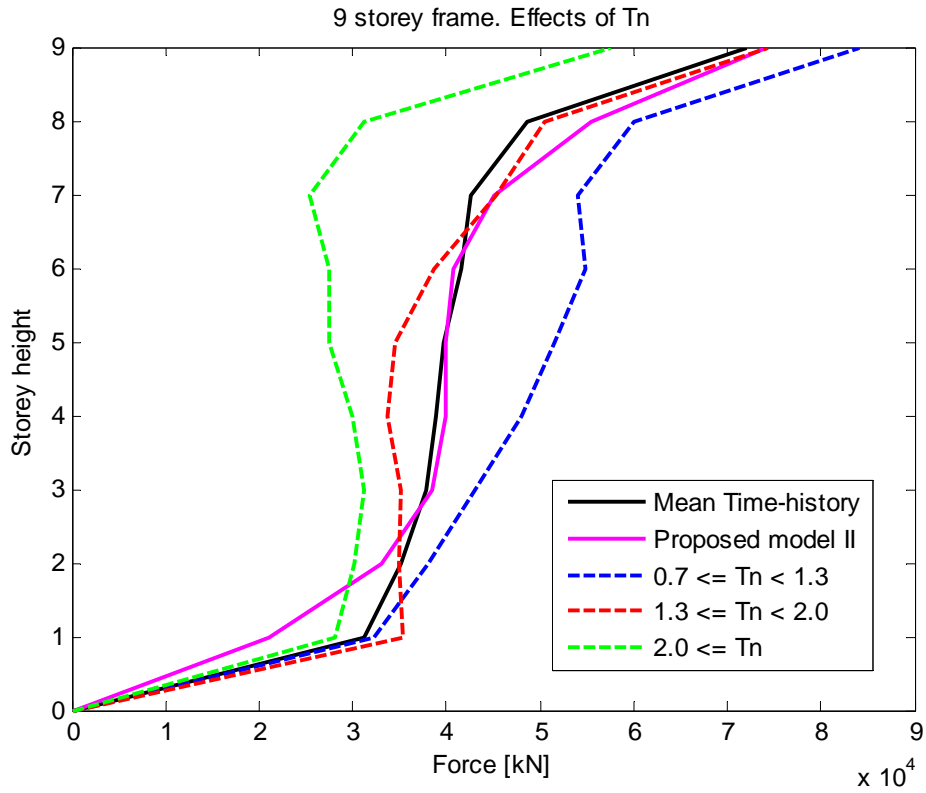


Figure 6.4: Proposed model II compared with the mean time-history results for the nine storey frame. Effects of T_n groups to the storey force response shown along.

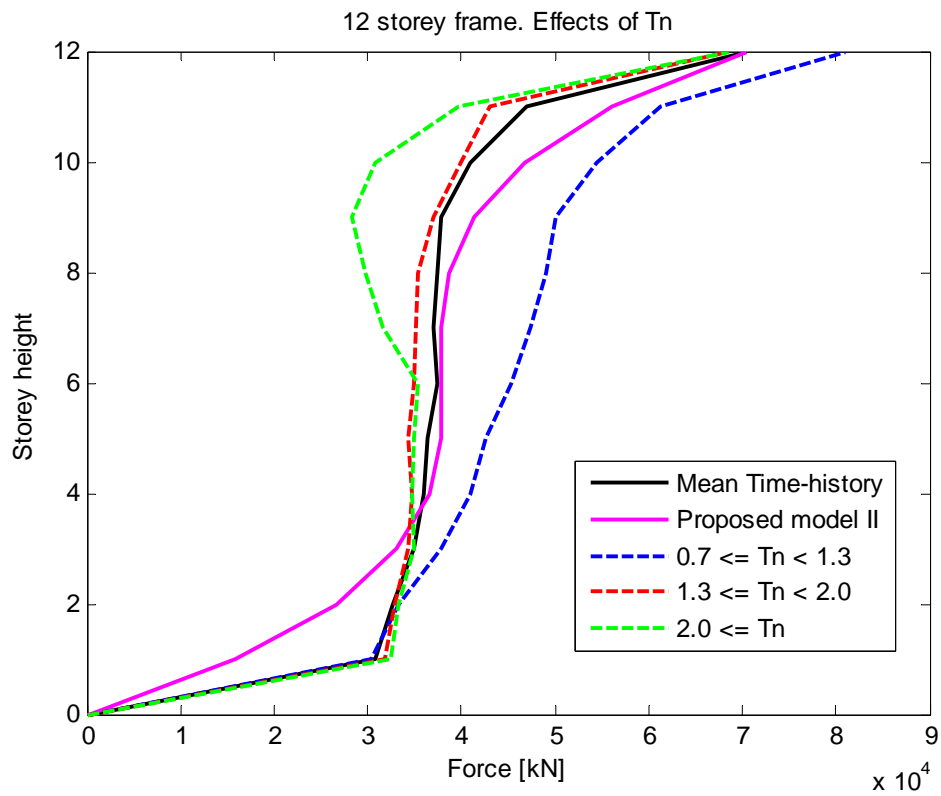


Figure 6.5: Proposed model II compared with the mean time-history results for the twelve storey frame. Effects of T_n groups to the storey force response shown along.

For the nine storey frame in Figure 6.4 the contribution of $0.7 \leq T_n < 1.3$ causes the highest forces to the mean time-history storey force response except on the first storey where the ground motions series group of $1.3 \leq T_n < 2.0$ contributes the highest force. The proposed model differs most from the mean time-history in the first storey and eight storey.

For the twelve storey frame in Figure 6.5 the group of $0.7 \leq T_n < 1.3$ causes the greatest force contribution to the mean time-history storey force response but all the groups are very close in the first storey. The proposed model differs from the mean time-history most in the first storey and eleventh storey.

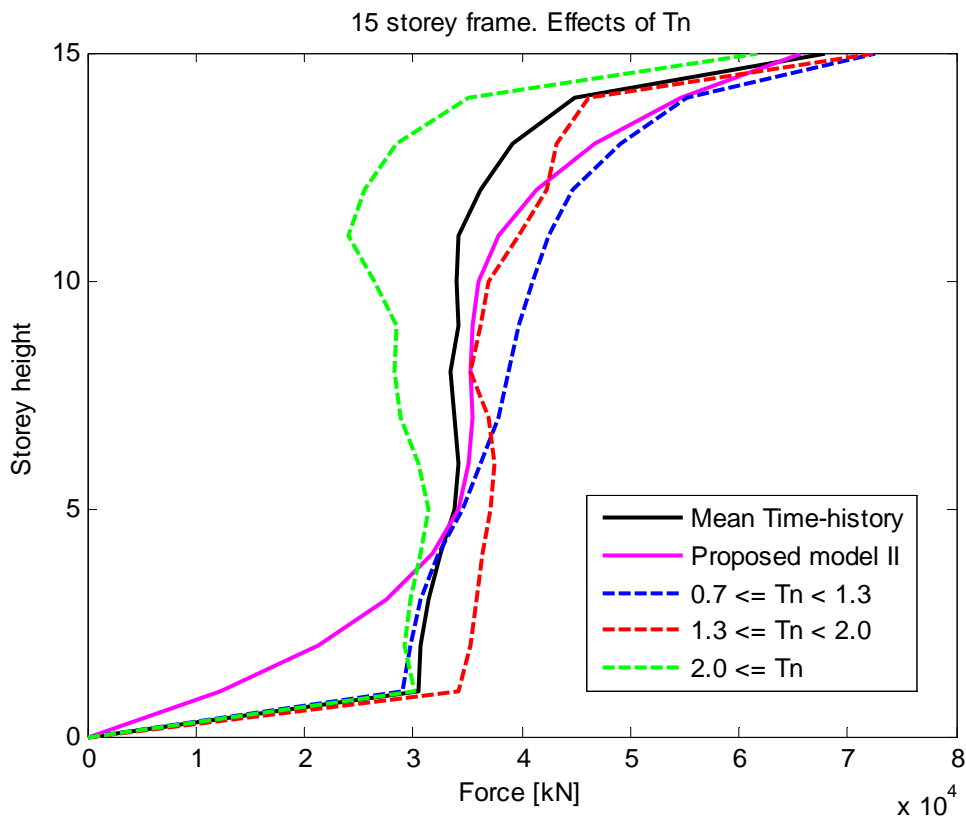


Figure 6.6: Proposed model II compared with the mean time-history results for the fifteen storey frame. Effects of T_n groups to the storey force response shown along.

For the fifteenth storey frame in Figure 6.6 the group of $1.3 \leq T_n < 2.0$ causes the highest force contribution to the mean time-history storey force response at storey one to seven but the group of $0.7 \leq T_n < 1.3$ causes the highest force contribution at storey eight to the top. The proposed model differs from the mean time-history most in the first storey and fourteenth storey.

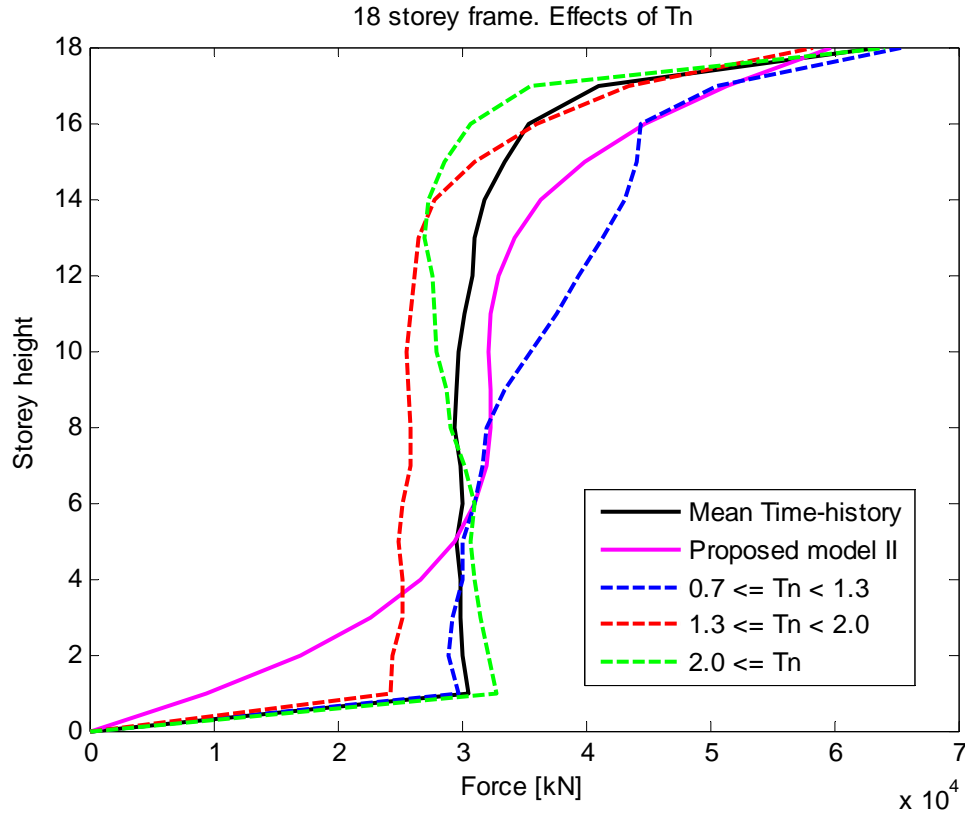


Figure 6.7: Proposed model II compared with the mean time-history results for the eighteen storey frame. Effects of T_n groups to the storey force response shown along.

For the eighteenth storey frame in Figure 6.7 the group of $2.0 \leq T_n$ causes the greatest force contribution to the mean time-history storey force response at storey one to five but the group of $0.7 \leq T_n < 1.3$ causes the greatest force contribution at storey six to the top. The proposed model differs most from the mean time-history in the first storey and seventeenth storey. For simplicity, the proposed model does not take into account the effect of normalized periods. The effect of normalized periods could be taken into account by calibrating new model parameters for each group of normalized periods.

6.1.2 Comparison of mean time-history results, proposed model II and EC8 provision

In this section the proposed model II is tested and compared with the near-fault time-history results along with the EC8 storey force method.

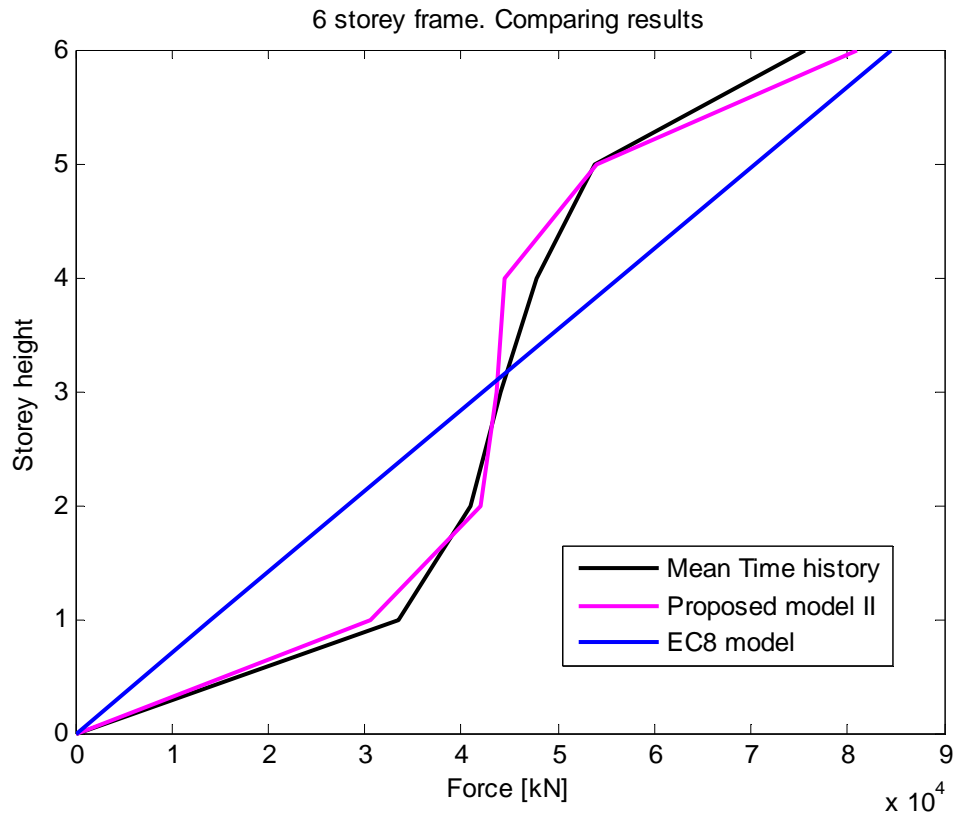


Figure 6.8: Proposed model II compared with the mean time-history results and EC8 storey force method.

For the six storey frame in Figure 6.8 it can be seen that the proposed model fits the mean time history storey forces better than the EC8 method.

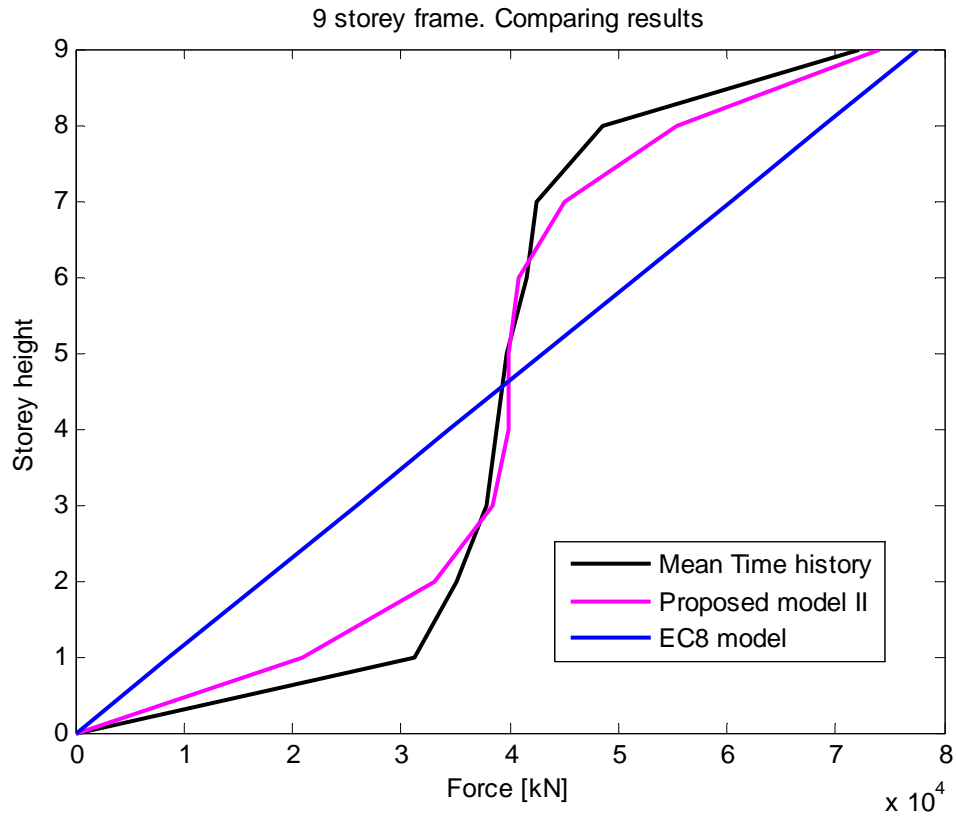


Figure 6.9: Proposed model II compared with the mean time-history results and EC8 storey force method.

For the nine storey frame in Figure 6.9 it can be seen that the proposed model starts to differ from the mean time history storey forces at the first and eight storey but simulates the response better than the EC8 method and this is the pattern observed for the 12, 15 and 18 storey frames too.

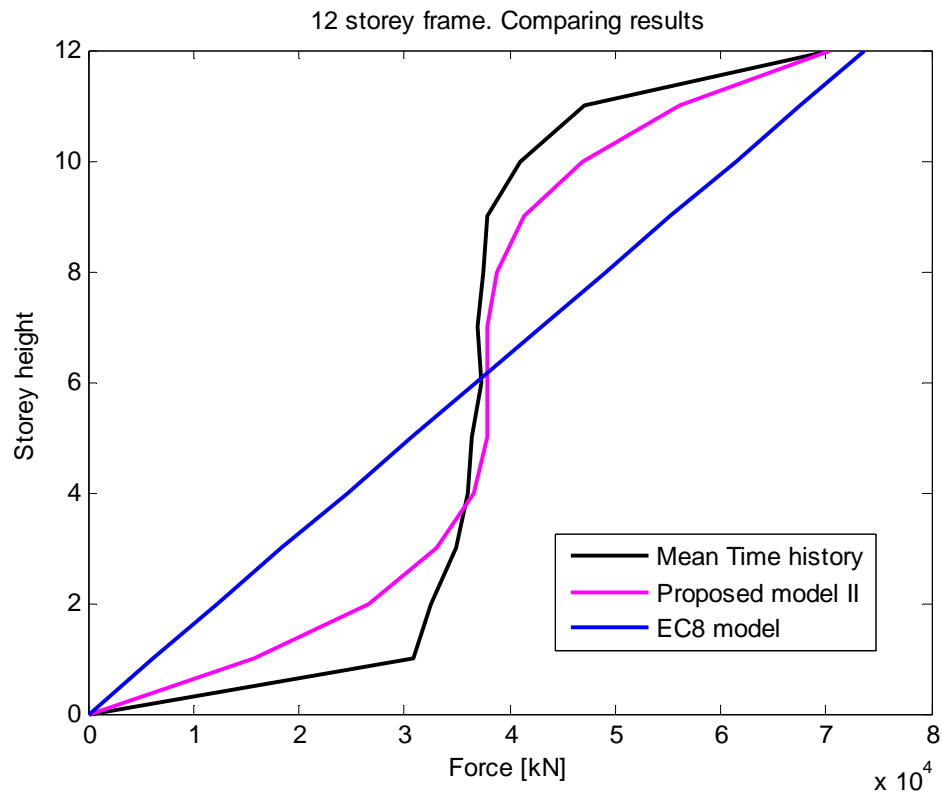


Figure 6.10: Proposed model II compared with the mean time-history results and EC8 storey force method.

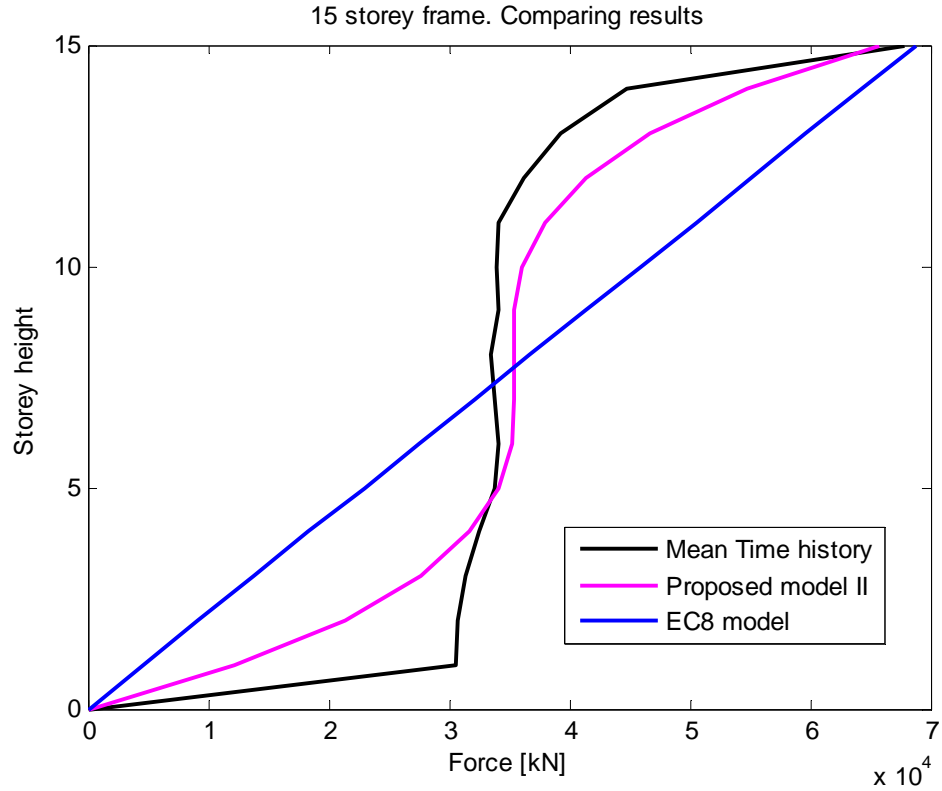


Figure 6.11: Proposed model II compared with the mean time-history results and EC8 storey force method.

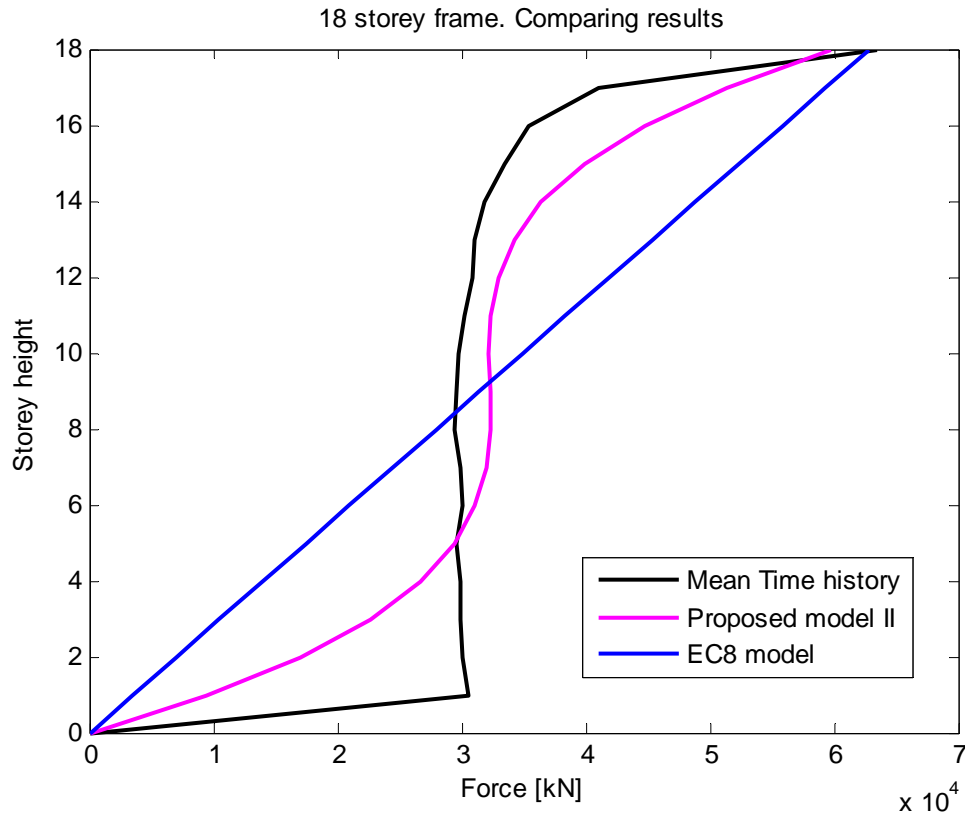


Figure 6.12: Proposed model II compared with the mean time-history results and EC8 storey force method.

For the eighteenth storey frame in Figure 6.12 it can be seen that although the difference between the proposed model and the mean time history storey forces is greater for this frame than all the other frames, the simulated response is considerably improved from the EC8 storey force method. The proposed model was obtained when fitted to the average of all the mean time-history storey forces and was simplified to a 3rd degree polynomial which cannot accurately simulate the high forces in the lowest first five storeys of the eighteenth storey frame but is still a step forward compared to the EC8 storey force method for near-fault areas.

7 Conclusions

The conclusions of this work are summarized here below in context with the objectives listed in section 1.2.

- The response of five elastic steel frames of different heights was analysed due to near-fault time-history ground motions. The structural systems used in this study are single-bay planar moment resisting steel frames. The properties of the modelled frames are the same as were used in Rupakhety (2008) which are based on the elastic properties model from Chintanapakdee and Chopra (2003) which has been used by researchers since. The time-history dataset used for the analysis was collected and processed by Rupakhety *et al.* (2010). Difference of maximum absolute shear forces in the columns gave the distribution of equivalent static storey forces along the height of the frames. The distribution of the equivalent static storey forces was different for all the frames due to the different modal vibration properties of the frames.
- The time-history distribution results of equivalent static storey forces for the frames differed increasingly from the linear distribution of equivalent static storey force method in EC8, as the total height increased. The EC8 storey force method approximates the dynamic behaviour by considering only a single mode. This suggest that for near-fault sites that the linear distribution of equivalent static storey force method in EC8 might not satisfy the possible near-fault storey forces for the lower half of tall structures but for the upper half of structures the provision is excessive based on these results. This means that in a strong near-fault ground motion a structure may experience excessive non-linear behaviour in the lower half of its total height but remain linear-elastic in the upper half of its total height if it were designed by considering only a single mode for horizontal storey forces as EC8 storey force method does (Equation 20 in this project).
- The effect of the normalized period ($T_n = \frac{T_1}{T_d}$) were studied where the time-history records were gathered into three groups ($0.7 \leq T_n < 1.3$; $1.3 \leq T_n < 2.0$; $2.0 \leq T_n$) depending on length of T_n . The first group ($0.7 \leq T_n < 1.3$) with T_n close to the fundamental period produced a distribution of storey forces which resembled response of the fundamental period T_1 . The first group contributed generally the highest storey forces as the effective modal mass is dominated by the first mode. The second and third group with higher T_n contributed generally higher storey forces as the total

height of the frames increased. This is because as the total height of the frames increases then the fundamental period (T_1) increases and the predominant pulse period (T_d) gets closer to the period of higher mode shapes of the taller frames which results with higher mode response.

- Two models were proposed for near-fault ground motion areas which were obtained by fitting a 5th and 3rd degree polynomials to the average of all the mean storey force distribution near-fault time-history results for the frames. Model I is a fifth order polynomial with a very good fit to the mean of all mean storey force results. Model II is a third order polynomial which doesn't fit as well as the model I but is simpler. Model II was selected for further analysis in this project due to its simplicity. In further analysis examples, the proposed model II was found to simulate the storey force distribution better than the EC8 storey force distribution method.
- According to the results of this project the hypothesis is true that: The equivalent static storey force distribution in EC8 which approximates the dynamic behaviour by considering only a single mode does not simulate the response for near-fault ground motions adequately.

7.1 Final remarks

Researchers are widely addressing issues of near-fault ground motions and related structural issues. The amount of quality near-fault site recorded data is increasing every year which will help researchers to expand the understanding and improve the state of the art.

Response of linear elastic frame structures were analysed to near-fault time history ground motions in this study. It is generally uneconomical to design structures to remain elastic under severe ground motion. To allow for non-linear behaviour that fully utilizes the capacity of the structure, seismic codes allow for a reduction of elastic design forces. However, as the elastic forces are still the basis of design, it is important that they simulate the expected seismic forces with reasonable accuracy. Near-fault ground motions differ from far-fault ground motions which require different approach in seismic design where the possible severe characteristics of near-fault ground motions are considered. Two proposals for a simple model to simulate the seismic force for linear elastic structures are proposed in this study but as databases accumulate, the models will improve the current practice and lead to safer and more economic design for structures in near-fault areas.

8 References

- Abrahamson, N. A. (2000). "Effects of rupture directivity in probabilistic seismic hazard analysis". Proc. of the 6th International Conf. on Seismic Zonation, Earthquake Engineering Research Institute, Palm Springs.
- Abrahamson, N. A., & Somerville, P. G. (1996). "Effects of the hanging wall and foot wall on ground motions recorded during the Northridge earthquake". Bull. Seism. Soc. Am. , 86, S93-S99.
- Alavi, B., & Krawinkler, H. (2004). "Behavior of moment-resisting frame structures subjected to near-fault ground motions". Earthquake Engineering Structural Dynamics, 33, 687-706.
- Benioff, H. (1955). "Mechanism and Strain Characteristics of the White Wolf Fault as Indicated by the Aftershock Sequence, Earthquakes in Kern County, California, During 1955(G.B. Oakeshott, ed.)". California Division of Mines Bulletin , No. 171,199-202.
- CEN. 2004. EN 1998 – 1:2004, Eurocode 8: Design of structures for earthquake resistance – part 1: General rules, seismic actions and rules for buildings. European Committee for Standardization.
- Chopra, A. K. (2007). Dynamics of Structure – Theory and Applications to Earthquake Engineering. (Third Edition),Prentice Hall, Englewood Cliffs, New Jersey.
- Chopra, A. K., & Chintanapakdee, C. (2003). "Evaluation of modal pushover analysis using generic frames". Earthquake Engng Struct Dyn. , 32, 417-442.
- Goel, R. K., & Chopra, A. K. (1997). "Period formulas for moment-resisting frame buildings". *Journal of Structural Engineering* , 123(11), 1454-1461.
- Hall, J. F., Heaton, T. H., Halling, M. W., & Wald, D. J. (1995). "Near-source ground motion and its effects on flexible buildings". Earthquake Spect , 11, 569-530.
- Houser, G. W., & Trifunac, M. D. (1967). "Analysis of accelerograms: Parkfield earthquake". Bull.Seism.Soc.Am. , 57, 1193-1220.
- IBC (2000). "2000 International Building Code". Falls Church: Virginia 2000: International Code Counsel.
- Iwan, W. D. (1997). "Drift spectrum: measure of demand for earthquake ground motions". J. Struct.Eng.ASCE , 123, 397-404.
- Kawase, H., & Aki, K. (1990). "Topography effect at the critical SV-wave incidence: possible explanation of damage pattern by the Whittier Narrows, California, earthquake of 1 October 1987". Bull. Seism.Soc.Am. , 18, 1-12.
- Mahin, S., Bertero, V., Chopra, A., & Collins, R. (1976). "Response of the Olive View Hospital Main Building During the San Fernando Earthquake". Earthquake Engineering Research Center University of California, Berkeley , Report No. UCB/EERC-76/22,Oct.1976.
- Mavroeidis, G. P., & Papageorgiou, A. S. (2000). "Analysis and simulation of the near-source motion recorded at Aigion during the Ms=6.2, June 15, 1995 Aigion earthquake(Greece)". Proc. of the Sixth Int. Conf. on Seismic Zonation(6ICSZ) , Palm Springs, California, 12-15 November 2000.

- Mavroeidis, G. P., & Papageorgiou, A. S. (2002). "Near-source strong ground motion: characteristics and design issues". Proc. of the Seventh U.S. National Conf. on Earthquake Engineering(7NCEE) , Boston, Massachusetts, 21-25 July 2002.
- Mavroeidis, G. P., Dong, G., & Papageorgiou, A. S. 2004. "Near-fault ground motions, and the response of elastic and inelastic single-degree-of-freedom systems". Earthquake Engineering and Structural Dynamics 33, 1023-1050.
- Newmark, N. M. (1959). "A Method of Computation for Structural Dynamics". Journal of the Engineering Mechanics Division (ASCE) , 85, 67-94.
- Rupakhety, R. (2008). MSc-Thesis – Evaluation of equivalent pulses to predict the inelastic response of generic frames subjected to near-fault ground motions. University of Pavia, Pavia Italy.
- Rupakhety, R. (2010). PhD-Thesis – Contemporary issues in earthquake engineering research: processing of accelerometric data, modeling of inelastic structural response, and quantification of near-fault effects. School of Engineering and Natural Science, University of Iceland, Reykjavík.
- Rupakhety, R. (2011). Structural Dynamics course handout teaching material.
- Rupakhety, R., Sigurðsson, S., Papageorgiou, A. S. & Sigbjörnsson, R. (2010). About response of structures to near-fault ground motions. Bulletin of Earthquake Engineering.
- Somerville, P. (1997). "Engineering characteristics of near fault ground motions". SMIP97 Seminar Proceedings .
- Somerville, P., Graves, N. F., & Abrahamson, N. A. (1997). "Modification of empirical strong ground motion attenuation relations to include the amplitude and duration effects of rupture directivity.". Seismol. Res. Lett , 68, 199-222.
- UBC. 1997. Uniform Building Code. In International Conference of Building Officials. Whittier, California.

9 Appendix:

Table 9.1: The near fault (56 records) dataset metadata. The dataset was collected and processed by Rupakhety *et al.* (2010)

WID	Location	Date	Faulting Mechanism	Mw	Station	Component	PGV (cm/s ²)	Effect	Hypocentral depth	EpiD (km)	HypD (km)	Joyner-Boore Dist. (km)	Closest Fault Distance (km)	Rupture velocity	vr/beta	s (km)	d (km)	c.tilde.prime	vs30	Td (s)
1	San Fernando, CA, USA	09 February 1971	RV	6,61	PCD	SN	116,5	FD	13,0	11,9	17,6	0,0	1,8	2,5	0,8	4,0	21,9	1,9	2016,1	1,153
2	Coyote lake, CA, USA	08 June 1979	SS	5,74	GA6	SN	51,5	FD	9,6	4,4	9,1	0,4	3,1	2,7	0,8	4,1	5,0	3,1	663,3	0,819
3	Imperial Valley, CA, USA	15 October 1979	SS	6,53	Aeropuerto Mexicali	SN	44,3	FD	10,0	2,5	10,3	0,0	0,3	2,7	0,9	2,0	10,1	3,5	274,5	1,600
4	Imperial Valley, CA, USA	15 October 1979	SS	6,53	Agrarias	SN	54,4	FD	10,0	2,6	10,3	0,0	0,7	2,7	0,9	2,4	10,0	3,2	274,5	1,877
5	Imperial Valley, CA, USA	15 October 1979	SS	6,53	Brawley airport	SN	36,12	FD	10,0	43,2	44,3	8,5	10,4	2,7	0,9	38,1	8,4	2,6	208,7	0,810
6	Imperial Valley, CA, USA	15 October 1979	SS	6,53	EC county center FF	SN	54,5	FD	10,0	29,1	30,7	7,3	7,3	2,7	0,9	27,6	10,1	2,2	192,1	1,254
7	Imperial Valley, CA, USA	15 October 1979	SS	6,53	EC Meloland Overpass FF	SN	115	FD	10,0	19,4	21,8	0,1	0,1	2,7	0,9	19,4	10,1	4,0	186,2	1,226
8	Imperial Valley, CA, USA	15 October 1979	SS	6,53	E10	SN	46,9	FD	10,0	26,3	28,1	6,2	6,2	2,7	0,9	25,1	10,1	2,3	202,9	1,093
10	Imperial Valley, CA, USA	15 October 1979	SS	6,53	E04	SN	77,9	FD	10,0	27,1	28,9	4,9	7,1	2,7	0,9	26,6	8,9	2,1	208,9	0,731
11	Imperial Valley, CA, USA	15 October 1979	SS	6,53	E05	SN	91,5	FD	10,0	27,8	29,5	1,8	4,0	2,7	0,9	27,7	9,4	2,7	205,6	0,709
12	Imperial Valley, CA, USA	15 October 1979	SS	6,53	E06	SN	111,9	FD	10,0	27,5	29,2	0,0	1,4	2,7	0,9	27,5	9,9	3,4	203,2	1,862
13	Imperial Valley, CA, USA	15 October 1979	SS	6,53	E07	SN	108,9	FD	10,0	27,6	29,4	0,6	0,6	2,7	0,9	27,5	10,1	3,7	210,5	1,460
14	Imperial Valley, CA, USA	15 October 1979	SS	6,53	E08	SN	48,5	FD	10,0	28,1	29,8	3,9	3,9	2,7	0,9	27,5	10,1	2,7	206,1	2,236
15	Imperial Valley, CA, USA	15 October 1979	SS	6,53	El Centro Differential Array	SN	59,6	FD	10,0	27,2	29,0	5,1	5,1	2,7	0,9	26,4	10,1	2,5	202,3	0,618
16	Imperial Valley, CA, USA	15 October 1979	SS	6,53	Holtville Post Office	SN	55,2	FD	10,0	19,8	22,2	5,5	7,7	2,7	0,9	18,9	8,8	1,8	202,9	1,102
17	Mammoth Lake-06	25 May 1980	SS	5,70	Long Valley Dam (Upper L. Abut)	SN	33,1	NA	5,0	14,2	15,0	NA	NA	NA	NA	NA	NA	NA	345,4	0,714
18	Irpina, Italy-01	23 November 1980	NM	6,90	Sturno	SN	41,5	FD	9,5	30,4	31,8	6,8	10,8	NA	NA	24,1	5,7	2,5	1000,0	2,270
24	Taiwan SMART1 (40)	20 May 1986	RV	6,30	SMART1 C00	SN	31,2	NA	15,8	68,2	70,0	NA	NA	NA	NA	NA	NA	NA	274,5	1,680
25	Taiwan SMART1 (40)	20 May 1986	RV	6,30	SMART1 M07	SN	36,1	NA	15,8	67,2	69,0	NA	NA	NA	NA	NA	NA	NA	274,5	0,831
26	Palm Springs, CA, USA	08 July 1986	OB	6,06	NPS	SN	73,64	FD	11,0	10,6	15,3	0,0	4,0	3,0	0,8	8,5	9,8	2,6	345,4	1,280
28	Whittier Narrows, CA, USA	10 October 1987	OB	5,99	DOW	SN	30,4	FD	14,6	16,0	21,7	15,0	20,8	2,6	0,8	5,0	0,2	0,9	271,9	1,960
29	Whittier Narrows, CA, USA	10 October 1987	OB	5,99	LB Orange Eve	SN	32,9	FD	14,6	20,7	25,3	19,8	24,5	2,6	0,8	5,0	0,2	0,9	270,2	0,627
30	Superstition Hills, CA, USA	24 November 1987	SS	6,54	PTS	SN	106,8	FD	9,0	16,0	18,4	1,0	1,0	2,5	0,8	16,0	9,0	3,3	348,7	1,820
32	Loma Prieta, CA, USA	17 October 1989	OB	6,93	Gilroy Array #2	SN	45,7	FD	17,5	29,8	34,5	10,4	11,1	2,8	0,8	20,0	14,5	3,3	270,8	1,540
34	Erzincan, Turkey	13 March 1992	SS	6,69	ERZ	SN	95,4	FD	9,0	9,0	12,7	0,0	4,8	3,0	NA	9,0	6,0	2,1	274,5	1,494
38	Northridge, CA, USA	17 January 1994	RV	6,70	JFA	SN	67,42	FD	17,5	13,0	21,8	0,0	5,4	2,9	0,8	1,8	19,5	2,4	373,1	1,449
42	Northridge, CA, USA	17 January 1994	RV	6,70	NWS	SN	87,75	FD	17,5	21,6	27,8	2,1	5,5	2,9	0,8	14,1	19,5	3,1	285,9	0,780
45	Northridge, CA, USA	17 January 1994	RV	6,70	SCG	SN	130,3	FD	17,5	13,1	21,9	0,0	5,4	2,9	0,8	1,2	19,5	2,5	251,2	0,770

Response of linear-elastic structures to Near-fault ground motion

WID	Location	Date	Faulting Mechanism	Mw	Station	Component	PGV (cm/s2)	Effect	Hypocentral depth	EpiD (km)	HypD (km)	Joyner-Boore Dist. (km)	Closest Fault Distance (km)	Rupture velocity	vr/beta	s (km)	d (km)	c.tilde.prime	vs30	Td (s)
46	Northridge, CA, USA	17 January 1994	RV	6,70	SCH	SN	116,6	FD	17,5	13,6	22,2	0,0	5,2	2,9	0,8	0,6	19,5	2,6	370,5	1,430
65	Yountville	03 September 2000	SS	5,00	Napa Fire Station #3	SN	42,93	NA	10,1	9,9	14,2	NA	NA	NA	NA	NA	NA	NA	271,4	1,575
66	Chi-Chi, Taiwan aftershock	20 September 1999	RV	6,20	CHY024	SN	33,1	FD	8,0	25,5	26,7	18,5	19,7	1,6	NA	5,5	6,5	2,4	427,7	1,006
67	Chi-Chi, Taiwan aftershock	20 September 1999	RV	6,20	CHY080	SN	70,31	FD	8,0	29,5	30,5	21,3	22,4	1,6	NA	5,5	6,5	3,4	553,4	0,870
68	Chi-Chi, Taiwan aftershock	20 September 1999	RV	6,20	TCU076	SN	58,9	FD	8,0	20,8	22,2	13,0	14,7	1,6	NA	4,5	6,5	3,5	615,0	1,119
69	Chi-Chi, Taiwan aftershock	25 September 1999	RV	6,30	CHY101	SN	36,4	FD	16,0	50,0	52,5	34,6	36,0	3,2	NA	15,0	12,0	2,6	258,9	0,682
70	Parkfield, CA, USA	27 June 1966	SS	6,19	CO2	SN	75,1	FD	10,0	31,0	32,6	6,3	6,3	2,6	0,7	24,9	10,0	3,7	184,8	1,061
71	Gazli, USSR	17 March 1976	RV	6,80	KAR	SN	65,3	FD	18,2	12,8	22,3	3,9	5,5	2,4	0,7	0,1	16,9	3,9	659,6	2,852
74	Mexicali Valley, Mexico	09 June 1980	SS	6,37	VCT	SN	76,9	FD	11,0	NA	NA	NA	3,0	NA	NA	NA	NA	NA	NA	2,544
75	Morgan Hill, CA, USA	24 April 1984	SS	6,19	HAL	SN	39,7	FD	8,5	3,9	9,4	3,5	3,5	2,6	0,8	0,5	8,0	1,9	281,6	2,663
76	Palm Springs, CA, USA	08 July 1986	OB	6,06	DSP	SN	29,7	FD	11,0	10,4	15,1	1,0	6,8	3,0	0,8	9,3	8,8	1,7	345,4	2,025
77	Superstition Hills, CA, USA	24 November 1987	SS	6,54	ELC	SN	52,0	FD	9,0	35,8	36,9	18,2	18,2	2,5	0,8	18,0	9,0	3,1	192,1	2,710
78	Loma Prieta, CA, USA	17 October 1989	OB	6,93	LGP	SN	103,2	FD	17,5	18,5	25,4	0,0	3,9	2,8	0,8	17,9	14,5	3,2	477,7	2,918
79	Loma Prieta, CA, USA	17 October 1989	OB	6,93	STG	SN	57,2	FD	17,5	27,2	32,4	7,6	8,5	2,8	0,8	20,0	14,5	3,5	370,8	2,583
80	Sierra Madre, CA, USA	28 June 1991	RV	5,56	COG	Rad (filt)	10,6	FD	NA	NA	NA	NA	9,4	NA	NA	NA	NA	NA	NA	1,570
88	South Iceland	17 June 2000	SS	6,57	Flagbjarnarholt	SN	72,2	FD	6,0	5,3	8,0	4,2	4,9	2,6	0,8	1,9	6,0	1,3	800,0	3,101
89	South Iceland	21 June 2000	SS	6,49	Thorsarbru	SN	79,7	FD	5,0	5,3	7,3	2,8	3,6	2,6	0,8	6,2	5,0	1,3	800,0	3,246
90	South Iceland	21 June 2000	SS	6,49	Thorsartun	SN	65,8	FD	5,0	5,6	7,5	3,6	2,9	2,6	0,8	6,2	5,0	1,5	800,0	3,423
91	South Iceland	21 June 2000	SS	6,49	Solheimar	SN	98,9	FD	5,0	11,0	12,1	4,1	4,6	2,6	0,8	9,9	5,0	1,7	560,0	3,321
92	Ólfus, South Iceland	25 May 2008	SS	6,30	EERC, Basement	SN	41,1	FD	5,0	8,0	9,4	3,3	6,2	2,6	0,8	4,9	5,0	1,3	800,0	3,031
93	Ólfus, South Iceland	25 May 2008	SS	6,30	Selkoss City Hall	SN	33,0	FD	5,0	8,0	9,4	3,3	6,2	2,6	0,8	4,9	5,0	1,3	800,0	3,054
94	Ólfus, South Iceland	25 May 2008	SS	6,30	Hveragerdi Retirement House	SN	54,0	FD	5,0	3,0	5,8	1,4	2,5	2,6	0,8	4,9	5,0	1,3	800,0	1,552
95	L'Aquila, Italy	06 April 2009	NM	6,30	AQK	SN	46,7	FD	NA	4,0	NA	0,0	NA	NA	NA	NA	NA	NA	580,0	3,449
96	Parkfield, CA, USA	28 September 2004	SS	6,00	Parkfield fault zone 12	SN	57,5	FD	8,1	11,1	13,7	0,9	0,9	2,6	0,8	23,4	8,1	1,4	339,0	3,808
97	Parkfield, CA, USA	28 September 2004	SS	6,00	Parkfield Cholame 2 west	SN	50,0	FD	8,1	11,5	14,1	1,9	1,9	2,6	0,8	10,0	8,1	3,3	185,0	4,016
99	Parkfield, CA, USA	28 September 2004	SS	6,00	Parkfield fault zone 1	SN	64,2	FD	8,1	8,4	11,7	0,0	0,0	2,6	0,8	8,4	8,1	4,0	339,0	3,986
100	Parkfield, CA, USA	28 September 2004	SS	6,00	Parkfield Cholame 3 west	SN	45,0	FD	8,1	11,9	14,4	2,5	2,5	2,6	0,8	10,0	8,1	3,1	339,0	4,236
106	Parkfield, CA, USA	28 September 2004	SS	6,00	Parkfield Cholame 1 east	SN	52,8	FD	8,1	11,6	14,1	1,9	1,9	2,6	0,8	10,0	8,1	3,3	339,0	4,100

